prepared and stained with Guava® Nexin reagent for 20 min and immediately processed with the Guava PCA system. Cells were gated based on forward scatter (size), and results reported as the percentage of gated cells positive for both annexin V and 7-AAD.

2.6. Immunoblot analyses

After treatment, cells were washed twice with ice-cold phosphate buffer saline (PBS), scraped with a cell scraper into ice-cold PBS and centrifuged at 1500 rpm for 10 min. The supernatant was removed and cell pellets were lysed with a RIPA buffer (Pierce Biotechnology, Rockford, Illinois, USA) containing a protease inhibitor (Pierce Biotechnology) for 15 min on ice. The insoluble matter was removed by centrifugation at 12,000 rpm for 20 min at 4 °C and supernatants were collected. Protein concentrations were determined with a Coomassie Plus™-The Better Bradford Assay Kit (Pierce Biotechnology).

Samples were mixed with 2× sample buffer (Bio-Rad Laboratories, Hercules, California USA) and heated for 5 min at 95 °C and then subjected to 10% SDS–PAGE. The separated proteins were transferred onto nitrocellulose membranes followed by blocking with 5% nonfat milk powder (w/v) in 1× TBS [10 mmol/L Tris–HCl (pH7.5), 100 mmol/L NaCl, 0.1% Tween-20] for 1 h at room temperature. Membranes were probed with antibodies for AR, Bax, cyclin D1, cyclin E, p21, p27, proliferating cell nuclear antigen (PCNA) (Santa Cruz Biotechnology, Inc., Santa Cruz, CA, USA), BcL-2, prostate-specific antigen (PSA) (DAKO, Denmark A/S, Glostrup, Denmark), CDK2, CDK4 (BD Biosciences, San Jose, CA, USA), Bad, Bcl-xL, caspase-3, cleaved caspase-3, poly(ADP-ribose) polymerase (PARP), p53, and survivin (Cell Signaling, Technology Inc., Danvers, Massachusetts, USA) in 5% nonfat dry milk, 1X TBS, 0.1% Tween-20 at 4 °C overnight, followed by exposure to peroxidase-conjugated appropriate secondary antibodies and visualization with an enhanced chemiluminescence detection system (GE Healthcare Bio-sciences, Buckinghamshire, NA, UK). To confirm equal protein loading, each membrane was stripped and reprobed with anti-β-actin (Sigma–Aldrich, Co., St. Louis, MO, USA) or anti-tubulin antibodies (Santa Cruz Biotechnology). Band density of Bad, Bax, Bcl-2, Bcl-xL and tubulin were then determined with ImageJ 1.410 (National Institute of Mental Health, Maryland, USA).

2.7. RNA interference

Cells were transfected with 20 nMol/L of control siRNA or two clones of siRNA for human p53 (Invitrogen, Carlsbad, CA, USA) using Lipofectamine™ RNAiMAX reagent (Invitrogen) for 24 h. p53 siRNA2 was used for subsequent experiments with BMLE or KuJ treatments.

2.8. Statistical analysis

All data are presented as mean ± S.D. values. Statistical analyses were conducted with Prism version 5.0 using one-way ANOVA, the Dunnett test or the Tukey's test. Statistical significance was concluded with *, **, ***: $P < 0.05$, 0.01 or 0.001, respectively.

3. Results

3.1. BMLE inhibits growth of LNCaP cells

LNCaP cells were treated with the varying concentrations (0–250 μg/ml) of BMLE for 24 h and 48 h, and its effects on cell growth were assessed by WST-1 assay. Cell growth of LNCaP was significantly inhibited by BMLE at between 25 and 250 μg/ml in a concentration-dependent manner. Inhibitory concentration (IC) 50 values were approximately 100 μg/ml and 50 μg/ml for 24 h and 48 h treatment, respectively (Fig. 1A).

3.2. BMLE induces cell cycle arrest in LNCaP cells

To explore the underlying mechanism of BMLE-induced growth suppression, cell cycle analysis was performed by Guava® cell cycle assay. BMLE-treated cells appeared to dramatically accumulate in G1 phase, especially at 150 (65%, $p < 0.01$), 200 (70%, $p < 0.001$) and 250 μg/ml (65%, $p < 0.01$), compared to control (52%), with concomitant decrease in the percentage of cells in the G2/M phase (Fig 1B and C). Cell cycle arrest began to occur from 24 h of treatment (data not shown). These results thus suggest that BMLE inhibited cell proliferation by arresting cells in the G1phase.

3.3. BMLE causes apoptotic death of LNCaP cells

In addition to cell cycle arrests, morphologic observation of BMLE-treated LNCaP cells indicated floating cells which are associated with cell death (data not shown). Guava® Nexin assays showed the treatment of LNCaP with 250 μg/ml of BMLE for 48 h resulted in significant increase in both the early and late stages of apoptosis (Fig. 1D): control (6% and 5%) and 250 μg/ml (24%, $P < 0.01$ and 34%, $P < 0.05$). It was shown that BMLE at high concentration caused inhibition of LNCaP cell growth by apoptosis induction.

3.4. Effects of BMLE on expression of cell cycle- and apoptosis-related proteins

LNCaP is an AR-positive prostate cancer cell line [27] expressing wild-type p53 [28]. As shown in Fig. 1E, BMLE (200 and 250 μg/ml) reduced its expression of AR and PSA proteins as assessed by western blotting analysis. Additionally, it was found that p53 protein expression was up-regulated after treatment with 250 μg/ml of BMLE, the concentration which caused both cell cycle arrest and induction of apoptosis.

As BMLE caused G1 arrest and apoptotic induction in LNCaP, we next examined the effect of BMLE on the expression of G1 cell cycle and apoptosis-regulatory proteins. Treatment with BMLE for 48 h also resulted in a marked reduction in the expression of cyclin D1 and PCNA in a concentration-dependent manner, as well as decrease in Bcl-2, with no effect on Bax. Besides, BMLE treatment led to the decrease of pro-caspase-3 and the increase of cleaved caspase-3 in a concentration-dependent manner (Fig. 1F). The cell cycle data shown in Fig. 1B and C coupled with the reduced expression of cyclin D1 and PCNA indicate that BMLE causes G1 arrest of LNCaP cells and the apoptosis data shown in Fig. 1F coupled with the decrease in Bcl-2 and the increase in cleaved caspase-3 indicate that BLME also induces LNCaP cells to undergo apoptosis. These data confirmed BMLE caused the inhibition of LNCaP cell growth via cell cycle arrest and apoptosis induction.

3.5. Identification of an active component in BMLE

According to Section 2, partition–extraction of BMLE using organic solvents (hexane, diethyl ether, chloroform and ethyl acetate) with increasing polarity provided four organic fractions. WST-1 assays showed growth inhibitory effects on LNCaP cells with all (Fig. 2A). The diethyl ether fraction (DEF) showed the strongest inhibitory effect on LNCaP cell growth (Fig. 2Ac), which led us to further isolate purified compound using DEF as a starting material.

The active compound in DEF was identified as KuJ (Fig. 2B), which we previously show its anti-cancer effect to modulate P-glycoprotein function and reverse cancer multidrug resistance [21,23], and this compound was further tested for influence on the growth of LNCaP cells (Fig. 2C). Treatment with KuJ for 24 h slightly decreased LNCaP cell growth, whereas treatment for 48 h significantly decreased cell growth and viability of the cancer cells with an IC50 of 15 μM.

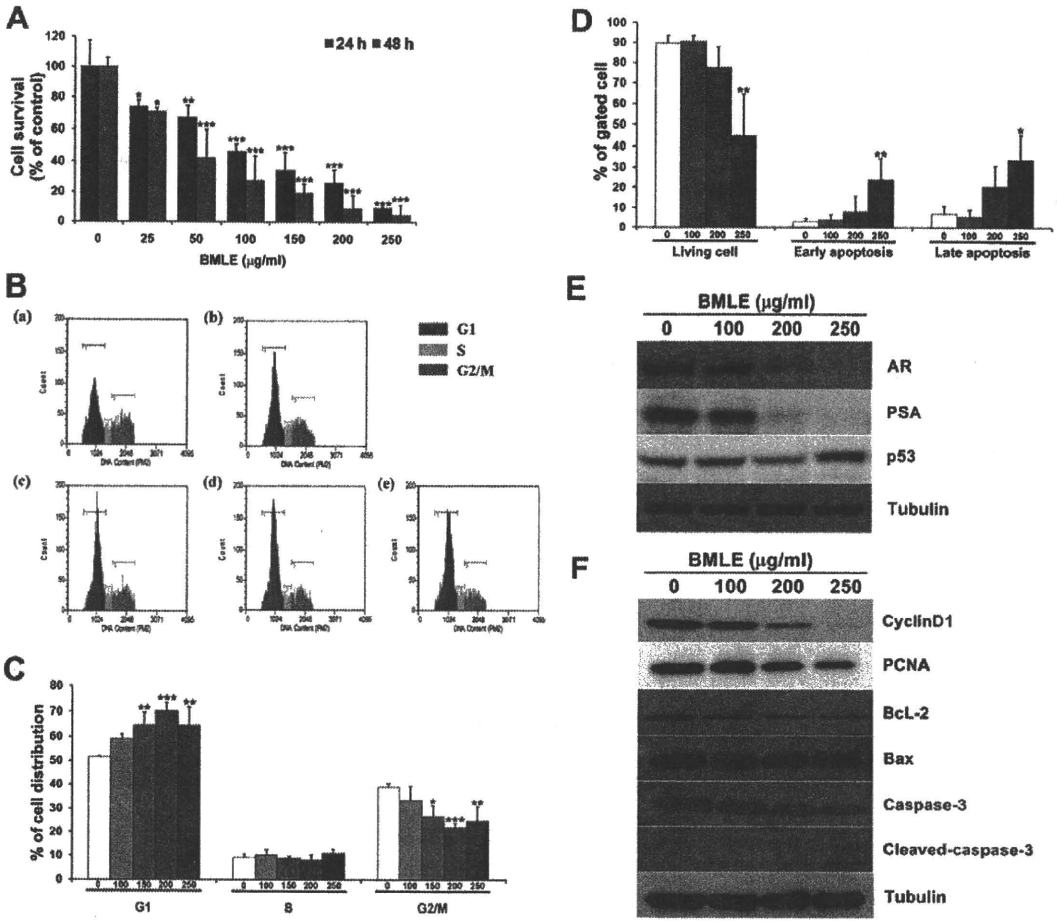

Fig. 1. BMLE caused G1 arrest and apoptosis induction in LNCaP cells. After incubation with 0–250 μg/ml BMLE for 24 and 48 h cytotoxicity was assessed by WST-1 assay (A). Histogram of cell cycle distribution (B) of LNCaP cells treated with vehicle control (a), 100 (b), 150 (c), 200 (d) and 250 (e) μg/ml BMLE for 48 h. Data analysis of cell cycle analyses (C) and apoptosis assays (D) of BMLE-treated LNCaP cells after 48 h of the treatment. The WST-1 results are expressed as percentages of vehicle control values. Data are mean ± SD values from three independent experiments. $^{*}P < 0.05$, $^{**}P < 0.01$ and $^{***}P < 0.001$, versus vehicle control. Immunoblot analysis of the protein levels of (E) AR, PSA, p53, (F) cell cycle-related proteins (cyclin D1 and PCNA) and apoptosis-related proteins (BcL-2, Bax, caspase-3 and cleaved-caspase-3) after treatment with vehicle control or BMLE for 48 h. The immunoblots shown here are representative of three independent experiments with similar results. Tubulin was employed as a loading control.

3.6. KuJ caused G1 cell cycle arrest in LNCaP cells

Based on the inhibitory effects of KuJ on LNCaP cell growth, the concentration of 15, 20, 25, and 30 μM of KuJ were selected for further *in vitro* mechanistic studies. As we found a significant effect of BMLE on cell cycle arrest in LNCaP, we thus determined the possible inhibitory effect of KuJ on cell cycle progression. As shown in Fig. 3A, treatment of LNCaP cells with KuJ for 24 and 48 h resulted in a significantly higher proportion of cells in the G1 phase at the concentrations used, 15 μM (67%, $p < 0.001$ and 64%, $p < 0.001$), 20 μM (70%, $p < 0.001$ and 69%, $p < 0.001$), 25 μM (64%, $p < 0.01$ and 63%, $p < 0.01$), and 30 μmol/L (59% and 64%, $p < 0.05$), compared with controls (55% and 53%). There was a concomitant reduction in the contributions of cells in the S and G2-M phases. These data suggest that inhibition of cell proliferation in LNCaP by KuJ might be associated with the induction of G1 arrest.

3.7. Induction of apoptosis by KuJ in LNCaP cells

To determine whether the KuJ-induced loss of the proliferation capacity and cell viability of LNCaP cells was associated with the induction of apoptosis, the cells were treated with KuJ as described above and the numbers of apoptotic cells were assessed. Apoptotic cells were counted as living cells and late or early apoptotic cells, which are presented in Fig. 3B. Treatment of KuJ for 24 h at 30 μM slightly but significantly induced apoptosis of LNCaP cells compare to controls (Fig. 3Ba). Treatment of LNCaP cells by 25 and 30 μM of KuJ for 48 h resulted in significant enhancement in the number of apoptotic cells in both the early and late stages of apoptosis (Fig. 3Bb): control (6% and 5%), 25 μM (33%, $P < 0.01$ and 15%, $P < 0.05$) and 30 μM (40%, $P < 0.01$ and 40%, $P < 0.001$).

3.8. Alteration of cell cycle- and apoptosis-related protein levels by KuJ

We next determined the expression of AR, PSA, and p53 and found that after 48 h treatment, KuJ reduced the protein expression of AR and PSA while enhancing the level of p53 in LNCaP cells in a concentration-dependent manner (Fig. 4A).

The expression of Cdk inhibitors, p21 and p27, which regulate the progression of cells in the G1 phase were assessed. Protein levels of p21 and p27 were increased following treatment with 15 and 20 μM KuJ for 48 h. On the other hand, the protein level of p21 was decreased, while the expression of p27 was still induced by treatment with 25 and 30 μM KuJ (Fig. 4B). Additionally, the expression of G1 positive regulators (cyclin D1, cyclin E, Cdk2, Cdk4 and PCNA) was down-regulated in a concentration-dependent manner (Fig. 4B).

We next determine whether the protein levels of apoptosis-involving proteins would be altered by KuJ. Treatment with KuJ at 15 and 20 μM resulted in a concentration-dependent reduction in the levels of the anti-apoptotic protein Bcl-xL with a concomitant increase in the level of pro-apoptotic protein Bad, while that of Bax was not changed (Fig. 4C). KuJ treatment at 25 and 30 μM dramatically decreased the protein

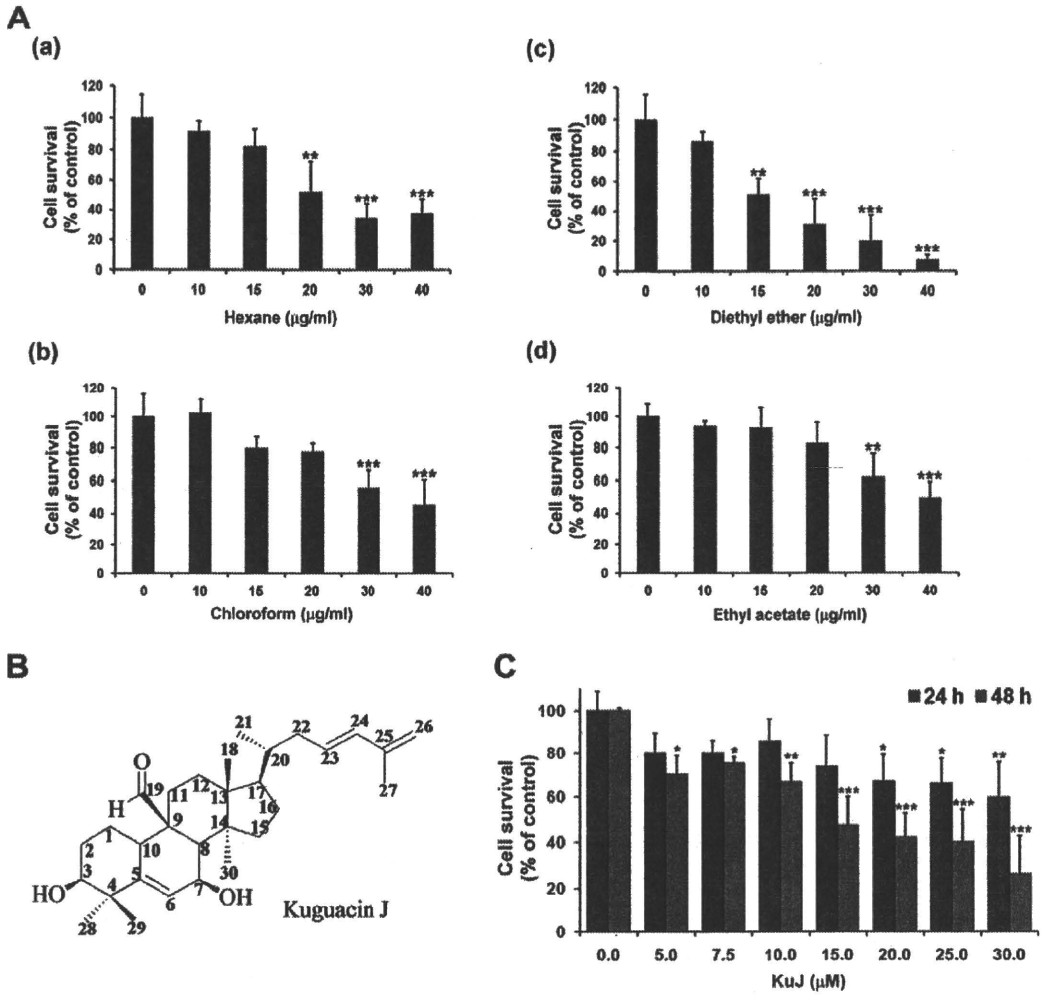

Fig. 2. Characterization of an active component in BMLE. (A) Cells were treated with 0–40 μg/ml of organic fractions obtained by partition–extraction using: (a) hexane, (b) diethyl ether, (c) chloroform and (d) ethyl acetate for 48 h and then WST-1 assays were perform to determine their growth inhibitory effects. (B) Structural formula of KuJ. (C) KuJ showed growth suppression in LNCaP cells as demonstrated by the WST-1 assay. The results are expressed as percentages of the vehicle control group value. Data are mean ± SD values from three independent experiments. $^{*}P < 0.05$, $^{**}P < 0.01$ and $^{***}P < 0.001$, versus control.

expression of Bcl-xL and Bcl-2 and slightly reduced the level of Bad and Bax. Band density analyses indicated that while KuJ treatment caused an overall decrease in expression of pro-apoptotic proteins, at the same time it elevated the ratios of Bax/Bcl-2 and Bad/Bcl-xL, which could initiate the caspase activation pathway for apoptosis (Data not shown) Likewise, KuJ treatment at dose of 25 and 30 μM, dramatically decreased the expression of survivin and caspase-3 and increased the expression of cleaved caspase-3 accompanied by cleavage of PARP.

The results demonstrated that KuJ altered the expressions of cell cycle- and apoptosis-regulatory proteins contributed to G1 arrest and apoptosis induction in LNCaP cells.

3.9. p53-dependent cell cycle arrest and apoptosis induction by KuJ in LNCaP cells

The induction of p53 might be a one possibility for BMLE and KuJ to trigger LNCaP cell growth. To investigate this mechanism, the cells were transfected with p53 siRNA follow by BMLE or KuJ treatment. The efficiency of p53 siRNA was proven with reference to decrease of p53 protein expression using western blotting analysis, and the expression of p21, a downstream target of p53 also was determined (Fig. 5A). In LNCaP cells, p53 protein expression was knocked down by treatment of p53 siRNA for 24 h compared with the control siRNA. Then the cells were treated with BMLE (250 μg/ml) or KuJ (25 μM) and the percentage cell distribution and apoptotic cell death were determined. As shown in Fig. 5B and C, transfection of p53 siRNA in LNCaP cells significantly reversed BMLE-induced cell cycle arrest, but slightly decreased KuJ-induced arrest of the cell cycle. Furthermore, the increase of the number of apoptotic cells by BMLE and KuJ was dramatically reduced when the cells were pre-treated with p53 siRNA (Fig. 5D and E).

3.10. Cytotoxicity of BMLE and KuJ in PNT1A cells

PNT1A cells were treated with various concentrations of BMLE or KuJ for 24 h and 48 h, and cell viability were assessed by WST-1 assay. With BMLE treatment, the viability of the cells was significantly reduced at concentrations between 200 and 250 μg/ml. The IC 50 values for BMLE were approximately 100 μg/ml and 50 μg/ml for 24 h and 48 h treatment, respectively (Fig. 6A). Cell viability was significantly decreased by KuJ at concentrations between 25 and 30 μM for 24 h and 20–30 μM for 48 h treatment. The IC 50 was more than 30 μM for both 24 h and 48 h treatment, (Fig. 6B). In contrast to the effect of BMLE and KuJ in cancer cell line, LNCaP, the results showed that the both compounds caused less toxicity in non-neoplastic human prostate epithelial cells.

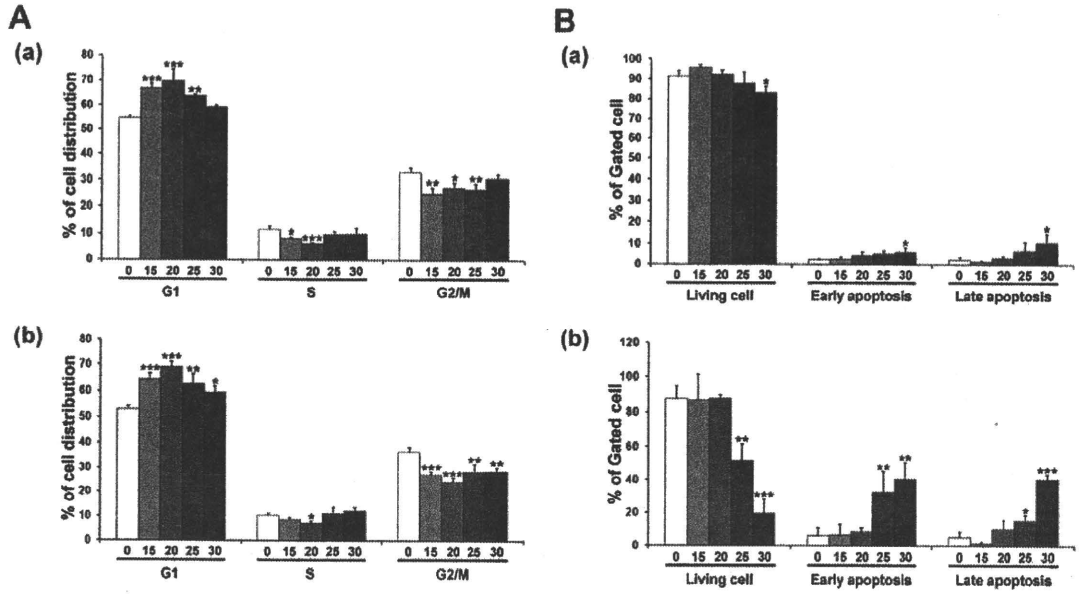

Fig. 3. Effects of KuJ on cell cycle progression and apoptosis induction in LNCaP cells. After treatment with 0, 15, 20, 25 and 30 μM KuJ, cells were harvested for analysis of cell cycle distribution and apoptosis. (A) LNCaP cell cycle distribution after treatment with KuJ for 24 (a) and 48 h (b). (B) Percentage of living cells, early and late apoptoses were summarized after 24 (a) and 48 h (b) of KuJ treatment. Data are mean ± SD values from three independent experiments. $^{*}P < 0.05$, $^{**}P < 0.01$ and $^{***}P < 0.001$, versus vehicle control.

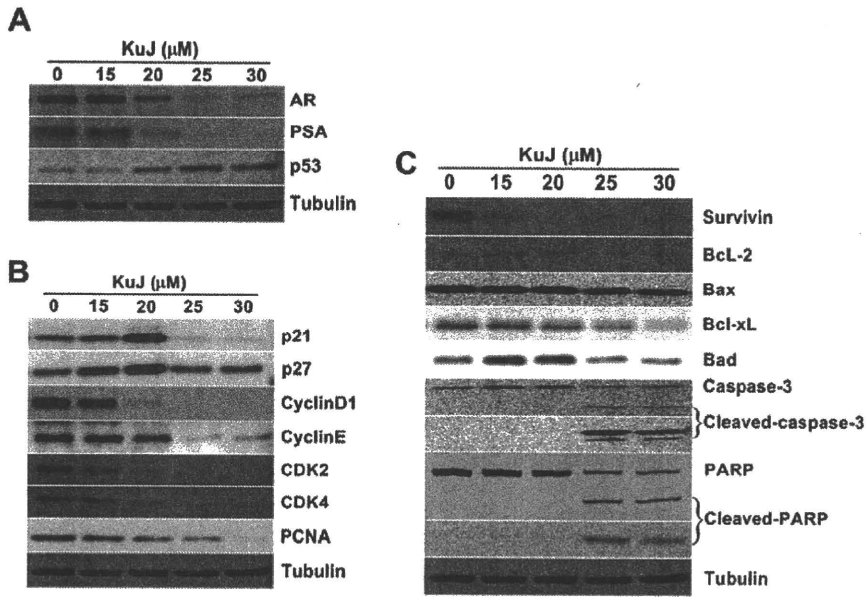

Fig. 4. KuJ alteration of the expression of cell cycle- and apoptosis-involving proteins. Immunoblot analysis of the protein levels of AR, PSA, p53 (A), cell cycle-related proteins (p21, p27, cyclin D1, cyclinE, CDK2, CDK4 and PCNA); (B) and apoptosis-related proteins (survivin, BcL-2, Bax, Bcl-xL, Bad, caspase-3, cleaved-caspase-3, PARP and cleaved-PARP); (C) after treatment with vehicle control or KuJ for 48 h. The immunoblots shown here are representative of three independent experiments with similar results. Tubulin was employed as a loading control.

4. Discussion

Fruits, vegetables, and common beverages, as well as several herbs and plants with diversified pharmacological properties, have been shown to be rich sources of micro-chemicals with the potential to prevent human cancers [29,30]. Prostate cancer is an ideal disease for chemopreventive intervention as it grows slowly before the onset of symptoms and the establishment of diagnosis, which usually occurs in men more than 50 years of age. Therefore, pharmacological or nutritional intervention could considerably impact the quality of life of patients by delaying the progression of cancer [5]. The present study found that BMLE exerted significant growth inhibitory

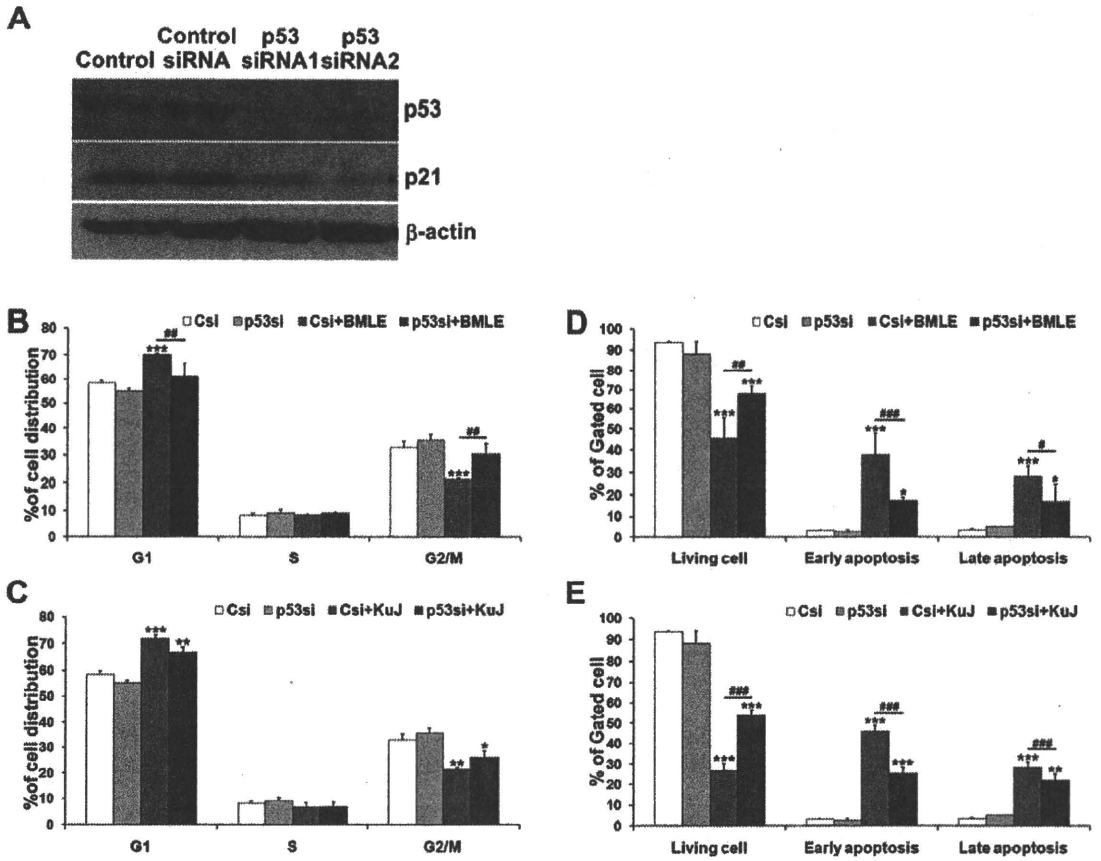

Fig. 5. BMLE and KuJ induction of p53-mediated cell cycle arrest and apoptosis in LNCaP. (A) Efficiency of p53 knockdown by 20 nM p53 siRNA was verified using Western blotting at 24 h post transfection. Cell cycle distribution and apoptosis were estimated when siRNA-transfected LNCaP cells were treated with (B and D) 250 μg/ml BMLE and (C and E) 25 μM KuJ. Data are mean ± SD values from three independent experiments. * or $^{\#}P < 0.05$, ** or $^{\#\#}P < 0.01$ and *** or $^{\#\#\#}P < 0.001$, versus control.

effects on LNCaP cells via induction of G1 arrest and apoptosis cell death. Thus identification of anti-cancer component(s) in BMLE could be valuable for prevention and intervention of cancers and the partition–extraction yielded four organic fractions, among which, DEF exerted the highest growth inhibitory effects. After the isolation using DEF as a starting material, KuJ, a known triterpenoid was obtained which also caused dramatic decrease of LNCaP cell proliferation and viability, indicating that it is at least one active component in BMLE.

Regulation of cell cycle progression in cancer cells is considered to be a potentially effective mechanism for control of tumor growth [31,32]. Molecular analyses of human cancers have revealed that cell cycle regulators frequently often display abnormalities in encoding genes in most common malignancies [33,34]. Here, treatment of androgen-sensitive (LNCaP) cells with KuJ resulted in significant G1-phase arrest of cell cycle progression, along with reduction of cyclin D1, cyclinE, Cdk2 and Cdk4 and increase of p21 and p27 at the protein level. This indicates the KuJ-induced G1 arrest might be mediated through the up-regulation of p21 and p27 proteins, which enhance the formation of heterotrimeric complexes with G1-S Cdks and cyclins, thereby inhibiting their activity. Additionally, KuJ also dramatically suppressed the expression of a proliferation marker, PCNA, that is expressed in late G1 phase and early S phase [35]. The inhibition of cell proliferation or the induction of cell death in LNCaP by KuJ might be associated with G1 arrest machinery.

G1-phase arrest of cell cycle progression provides an opportunity for cells to either undergo repair or follow the apoptotic pathway, which plays a crucial role in tissue homeostatic eliminating mutated hyperproliferating neoplastic cells from the system. Acquired resistance toward apoptosis is a hallmark of most and perhaps all types of cancer. Therefore induction of apoptosis is considered to be one of protective mechanisms against cancer progression. In the present study, treatment of LNCaP cells with 25 and 30 μM of KuJ resulted in significant induction of apoptosis. Survivin is a member of the inhibitor of apoptosis protein family, involved in inhibition of apoptosis, exerts multiple effects throughout the cell cycle [36]. Our study revealed that KuJ treatment reduced the protein level of survivin, which might be associated with KuJ-induced cell cycle arrest and apoptosis in LNCaP cells. In addition, since the ratios of pro-apoptotic proteins (e.g., Bad and Bax) and anti-apoptotic proteins (e.g., Bcl-2 and Bcl-xL) are essential for the regulation of apoptosis through

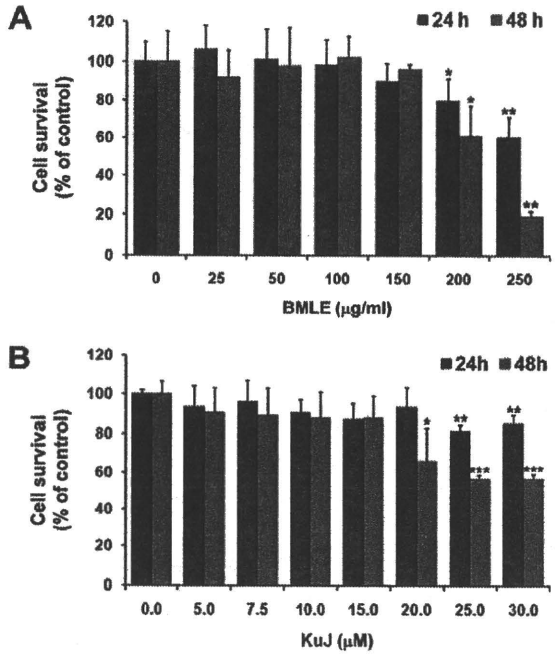

Fig. 6. Cytotoxicity of BMLE and KuJ in PNT1A cells. Cells were incubated with (A) 0–250 μg/ml BMLE or (B) 0–30 μM KuJ for 24 and 48 h and then cytotoxicity was assessed by WST-1 assay. The WST-1 results are percentages of vehicle control values. Data are mean ± SD values from three independent experiments. $^{*}P < 0.05$, $^{**}P < 0.01$ and $^{***}P < 0.001$, versus control.

caspase signaling [37], the finding that KuJ could alter the protein levels of key members of the Bcl-2 family in a manner that favors an increase in the ratios of Bax/Bcl-2 and Bad/Bcl-xLis of obvious significance.

AR is known to play a critical role in the development and progression of prostate cancer through alteration of the normal androgen axis by dysregulation of AR activity [38]. An ability of AR to cross-talk with several growth factor signaling cascades active regulation of cell cycle, apoptosis, and differentiation outcomes in prostate cancer cells has been reported [39]. The fact that KuJ decreased the expression of AR followed by reduction of protein level of PSA might be involved in KuJ-caused growth inhibition of LNCaP through the induction of G1 arrest and apoptosis.

The tumor suppressor p53 protein is a regulator of genotoxic stress that plays an important role in DNA damage response, DNA repair, cell cycle regulation, and in triggering apoptosis after cell injury [40]. Induction of apoptosis is considered to be a central to the tumor-suppressive function of p53 [41]. Knockdown of p53 by RNA interference in LNCaP slightly suppressed cell cycle arrest whereas it markedly abolished apoptosis induction by KuJ. These results indicate that KuJ induced p53-mediated partly cell cycle arrest and mainly apoptosis, which led to the inhibition of cell growth, and may be related with the activation of p53 signaling pathways.

Because KuJ was purified from BMLE, the two were compared. The growth inhibition effects of KuJ on LNCaP cells proved similar to those of BMLE. However, KuJ accounts for only approximately 1.6% of BMLE, and the effective concentration of KuJ was only 10-fold lower. Therefore, BMLE may include other compounds which also exert anti-tumor effects. Cucurbitacin B (cucB), a triterpenoid from Cucurbitaceae vegetables also found in bitter melon seeds, caused cell cycle arrest and apoptosis induction in human colon adenocarcinoma cancer cells [42]. Additionally, Rutin, a flavonoid present in bitter melon leaves, has been reported to show growth inhibition of leukemia and ovarian carcinoma cells, with anti-invasive effects on melanoma cells [43–46]. Therefore characterization of other active components present in BMLE has to be further explored.

Interestingly, the sensitivity of the human normal prostatic epithelial cell line, PNT1A, to the cytotoxic effects of BMLE and KuJ was much lower than that of LNCaP cells, pointing to potential use as effective chemopreventive agents against androgen-sensitive prostate cancer cells. In Asia people consume fruit and/or leaves of bitter melon as food [6,7] and this and other components of the diet may be linked to low incidences of prostate cancer in general [47].We have reported BMLE to inhibit the progression of androgen-independent rat prostate cancers *in vitro* and *in vivo* [19]. To provide a basis for use of KuJ as a broader antineoplastic agent for prostate cancer, further study is needed to investigate anti-cancer effects of KuJ on human androgen-independent prostate cancer.

In conclusion, we here report for the first time the ability of BMLE and KuJ to inhibit cell proliferation and viability through induction of G1-phase arrest and apoptosis on an androgen-dependent human prostate cancer cell line, while exhibiting only low toxicity in normal human prostate epithelial cells. In addition, we provide mechanistic evidence that KuJ-induced G1 arrest and apoptosis in prostate carcinoma cells might be partly mediated through enhanced expression of p53. Taking the results together, KuJ might be a promising candidate new chemopreventive agent for androgen-dependent prostate cancer.

Conflicts of interest

None declared.

Acknowledgment

This work was supported by grants from the Royal Golden Jubilee Ph.D. Program of Thailand, National Research Council of Thailand and the Society for Promotion of Pathology of Nagoya, Japan.

References

[1] H. Gronberg, Prostate cancer epidemiology, Lancet 361 (2003) 859–864.
[2] E. Bidoli, R. Talamini, C. Bosetti, E. Negri, D. Maruzzi, M. Montella, S. Franceschi, C. La Vecchia, Macronutrients, fatty acids, cholesterol and prostate cancer risk, Ann. Oncol. 16 (2005) 152–157.
[3] G.J. Kelloff, J.A. Crowell, V.E. Steele, R.A. Lubet, C.W. Boone, W.A. Malone, E.T. Hawk, R. Lieberman, J.A. Lawrence, L. Kopelovich, I. Ali, J.L. Viner, C.C. Sigman, Progress in cancer chemoprevention, Ann. N. Y. Acad. Sci. 889 (1999) 1–13.
[4] Y.J. Surh, Cancer chemoprevention with dietary phytochemicals, Nat. Rev. Cancer 3 (2003) 768–780.

[5] D.N. Syed, N. Khan, F. Afaq, H. Mukhtar, Chemoprevention of prostate cancer through dietary agents: progress and promise, Cancer Epidemiol. Biomarkers Prev. 16 (2007) 2193–2203.
[6] E. Basch, S. Gabardi, C. Ulbricht, Bitter melon (*Momordica charantia*): a review of efficacy and safety, Am. J. Health Syst. Pharm. 60 (2003) 356–359.
[7] A. Gurib-Fakim, A.H. Subratty, F. Mahomoodally, Bitter melon: an exotic vegetable with medicinal values, Nutr. Food Sci. 35 (2005) 143–147.
[8] F. Licastro, C. Franceschi, L. Barbieri, F. Stirpe, Toxicity of *Momordica charantia* lectin and inhibitor for human normal and leukaemic lymphocytes, Virchows Arch. B Cell Pathol. Incl. Mol. Pathol. 33 (1980) 257–265.
[9] T.B. Ng, W.K. Liu, S.F. Sze, H.W. Yeung, Action of alpha-momorcharin, a ribosome inactivating protein, on cultured tumor cell lines, Gen. Pharmacol. 25 (1994) 75–77.
[10] M.G. Battelli, L. Polito, A. Bolognesi, L. Lafleur, Y. Fradet, F. Stirpe, Toxicity of ribosome-inactivating proteins-containing immunotoxins to a human bladder carcinoma cell line, Int. J. Cancer 65 (1996) 485–490.
[11] C. Ganguly, S. De, S. Das, Prevention of carcinogen-induced mouse skin papilloma by whole fruit aqueous extract of *Momordica charantia*, Eur. J. Cancer Prev. 9 (2000) 283–288.
[12] Y. Sun, P.L. Huang, J.J. Li, Y.Q. Huang, L. Zhang, S. Lee-Huang, Anti-HIV agent MAP30 modulates the expression profile of viral and cellular genes for proliferation and apoptosis in AIDS-related lymphoma cells infected with Kaposi's sarcoma-associated virus, Biochem. Biophys. Res. Commun. 287 (2001) 983–994.
[13] H. Shi, M. Hiramatsu, M. Komatsu, T. Kayama, Antioxidant property of Fructus Momordicae extract, Biochem. Mol. Biol. Int. 40 (1996) 1111–1121.
[14] S. Lee-Huang, P.L. Huang, H.C. Chen, A. Bourinbaiar, H.I. Huang, H.F. Kung, Anti-HIV and anti-tumor activities of recombinant MAP30 from bitter melon, Gene 161 (1995) 151–156.
[15] M.J. Tan, J.M. Ye, N. Turner, C. Hohnen-Behrens, C.Q. Ke, C.P. Tang, T. Chen, H.C. Weiss, E.R. Gesing, A. Rowland, D.E. James, Y. Ye, Antidiabetic activities of triterpenoids isolated from bitter melon associated with activation of the AMPK pathway, Chem. Biol. 15 (2008) 263–273.
[16] J.E. Cunnick, K. Sakamoto, S.K. Chapes, G.W. Fortner, D.J. Takemoto, Induction of tumor cytotoxic immune cells using a protein from the bitter melon (*Momordica charantia*), Cell. Immunol. 126 (1990) 278–289.
[17] W.R. Kusamran, A. Ratanavila, A. Tepsuwan, Effects of neem flowers, Thai and Chinese bitter gourd fruits and sweet basil leaves on hepatic monooxygenases and glutathione S-transferase activities, and in vitro metabolic activation of chemical carcinogens in rats, Food Chem. Toxicol. 36 (1998) 475–484.
[18] P. Limtrakul, O. Khantamat, K. Pintha, Inhibition of P-glycoprotein activity and reversal of cancer multidrug resistance by *Momordica charantia* extract, Cancer Chemother. Pharmacol. 54 (2004) 525–530.
[19] P. Pitchakarn, K. Ogawa, S. Suzuki, S. Takahashi, M. Asamoto, T. Chewonarin, P. Limtrakul, T. Shirai, *Momordica charantia* leaf extract suppresses rat prostate cancer progression in vitro and in vivo, Cancer Sci. 101 (2010) 2234–2240.
[20] R.B. Ray, A. Raychoudhuri, R. Steele, P. Nerurkar, Bitter melon (*Momordica charantia*) extract inhibits breast cancer cell proliferation by modulating cell cycle regulatory genes and promotes apoptosis, Cancer Res. 70 (2010) 1925–1931.
[21] P. Pitchakarn, S. Ohnuma, K. Pintha, W. Pompimon, S. Ambudkar, P. Limtrakul, Kuguacin J isolated from *Momordica charantia* leaves inhibits P-glycoprotein (ABCB1)-mediated multidrug resistance, J. Nutr. Biochem., in press, doi:10.1016/j.jnutbio.2010.11.005.
[22] J. Chen, R. Tian, M. Qiu, L. Lu, Y. Zheng, Z. Zhang, Trinorcucurbitane and cucurbitane triterpenoids from the roots of *Momordica charantia*, Phytochemistry 69 (2008) 1043–1048.
[23] J.C. Chen, W.Q. Liu, L. Lu, M.H. Qiu, Y.T. Zheng, L.M. Yang, X.M. Zhang, L. Zhou, Z.R. Li, Kuguacins F-S, cucurbitane triterpenoids from *Momordica charantia*, Phytochemistry 70 (2009) 133–140.
[24] D.B. Mekuria, T. Kashiwagi, S. Tebayashi, C.S. Kim, Cucurbitane triterpenoid oviposition deterrent from *Momordica charantia* to the leafminer, *Liriomyza trifolii*, Biosci. Biotechnol. Biochem. 69 (2005) 1706–1710.
[25] N. Puspawati, Isolation and identification momordicin I from leaves extract of *Momordica charantia* L., J. KIMIA 2 (2008) 53–56.
[26] K. Hamasaki, K. Kogure, K. Ohwada, A biological method for the quantitative measurement of tetrodotoxin (TTX): tissue culture bioassay in combination with a water-soluble tetrazolium salt, Toxicon 34 (1996) 490–495.
[27] J.S. Horoszewicz, S.S. Leong, E. Kawinski, J.P. Karr, H. Rosenthal, T.M. Chu, E.A. Mirand, G.P. Murphy, LNCaP model of human prostatic carcinoma, Cancer Res. 43 (1983) 1809–1818.
[28] M. Burchardt, T. Burchardt, A. Shabsigh, M. Ghafar, M.W. Chen, A. Anastasiadis, A. de la Taille, A. Kiss, R. Buttyan, Reduction of wild type p53 function confers a hormone resistant phenotype on LNCaP prostate cancer cells, Prostate 48 (2001) 225–230.
[29] R.L. Thangapazham, A. Sharma, R.K. Maheshwari, Multiple molecular targets in cancer chemoprevention by curcumin, AAPS J. 8 (2006) E443–E449.
[30] N. Khan, V.M. Adhami, H. Mukhtar, Apoptosis by dietary agents for prevention and treatment of prostate cancer, Endocr. Relat. Cancer 17 (2010) R39–52.
[31] N.P. Pavletich, Mechanisms of cyclin-dependent kinase regulation: structures of Cdks, their cyclin activators, and Cip and INK4 inhibitors, J. Mol. Biol. 287 (1999) 821–828.
[32] R. Agarwal, Cell signaling and regulators of cell cycle as molecular targets for prostate cancer prevention by dietary agents, Biochem. Pharmacol. 60 (2000) 1051–1059.
[33] M. Nakanishi, M. Shimada, H. Niida, Genetic instability in cancer cells by impaired cell cycle checkpoints, Cancer Sci. 97 (2006) 984–989.
[34] W.K. Kaufmann, K.R. Nevis, P. Qu, J.G. Ibrahim, T. Zhou, Y. Zhou, D.A. Simpson, J. Helms-Deaton, M. Cordeiro-Stone, D.T. Moore, N.E. Thomas, H. Hao, Z. Liu, J.M. Shields, G.A. Scott, N.E. Sharpless, Defective cell cycle checkpoint functions in melanoma are associated with altered patterns of gene expression, J. Invest. Dermatol. 128 (2008) 175–187.
[35] G.L. Moldovan, B. Pfander, S. Jentsch, PCNA, the maestro of the replication fork, Cell 129 (2007) 665–679.
[36] D.C. Altieri, Survivin, versatile modulation of cell division and apoptosis in cancer, Oncogene 22 (2003) 8581–8589.
[37] V. Kirkin, S. Joos, M. Zornig, The role of Bcl-2 family members in tumorigenesis, Biochim. Biophys. Acta 1644 (2004) 229–249.
[38] C.A. Heinlein, C. Chang, Androgen receptor in prostate cancer, Endocr. Rev. 25 (2004) 276–308.
[39] M.L. Zhu, N. Kyprianou, Androgen receptor and growth factor signaling cross-talk in prostate cancer cells, Endocr. Relat. Cancer 15 (2008) 841–849.
[40] L.M. Rozan, W.S. El-Deiry, p53 downstream target genes and tumor suppression: a classical view in evolution, Cell Death Differ. 14 (2007) 3–9.
[41] K. Polyak, Y. Xia, J.L. Zweier, K.W. Kinzler, B. Vogelstein, A model for p53-induced apoptosis, Nature 389 (1997) 300–305.
[42] S. Yasuda, S. Yogosawa, Y. Izutani, Y. Nakamura, H. Watanabe, T. Sakai, Cucurbitacin B induces G(2) arrest and apoptosis via a reactive oxygen species-dependent mechanism in human colon adenocarcinoma SW480 cells, Mol. Nutr. Food Res. (2009).
[43] J.P. Lin, J.S. Yang, C.C. Lu, J.H. Chiang, C.L. Wu, J.J. Lin, H.L. Lin, M.D. Yang, K.C. Liu, T.H. Chiu, J.G. Chung, Rutin inhibits the proliferation of murine leukemia WEHI-3 cells in vivo and promotes immune response in vivo, Leuk. Res. 33 (2009) 823–828.
[44] H. Luo, B.H. Jiang, S.M. King, Y.C. Chen, Inhibition of cell growth and VEGF expression in ovarian cancer cells by flavonoids, Nutr. Cancer 60 (2008) 800–809.
[45] C. Martinez Conesa, V. Vicente Ortega, M.J. Yanez Gascon, M. Alcaraz Banos, M. Canteras Jordana, O. Benavente-Garcia, J. Castillo, Treatment of metastatic melanoma B16F10 by the flavonoids tangeretin, rutin, and diosmin, J. Agric. Food Chem. 53 (2005) 6791–6797.
[46] M. Zhang, N.S. Hettiarachchy, R. Horax, P. Chen, K.F. Over, Effect of maturity stages and drying methods on the retention of selected nutrients and phytochemicals in bitter melon (*Momordica charantia*) leaf, J. Food Sci. 74 (2009) C441–448.
[47] C.S. Muir, J. Nectoux, J. Staszewski, The epidemiology of prostatic cancer. Geographical distribution and time-trends, Acta Oncol. 30 (1991) 133–140.

Vol 464|29 April 2010|doi:10.1038/nature08991

ARTICLES

Adiponectin and AdipoR1 regulate PGC-1α and mitochondria by Ca^{2+} and AMPK/SIRT1

Masato Iwabu[1,2]*, Toshimasa Yamauchi[1,2]*, Miki Okada-Iwabu[1,2]*, Koji Sato[6], Tatsuro Nakagawa[7], Masaaki Funata[1], Mamiko Yamaguchi[1], Shigeyuki Namiki[3], Ryo Nakayama[1], Mitsuhisa Tabata[8], Hitomi Ogata[9], Naoto Kubota[1], Iseki Takamoto[1], Yukiko K. Hayashi[10], Naoko Yamauchi[4], Hironori Waki[1], Masashi Fukayama[4], Ichizo Nishino[10], Kumpei Tokuyama[9], Kohjiro Ueki[1], Yuichi Oike[8], Satoshi Ishii[5], Kenzo Hirose[3], Takao Shimizu[5], Kazushige Touhara[6,7] & Takashi Kadowaki[1]

Adiponectin is an anti-diabetic adipokine. Its receptors possess a seven-transmembrane topology with the amino terminus located intracellularly, which is the opposite of G-protein-coupled receptors. Here we provide evidence that adiponectin induces extracellular Ca^{2+} influx by adiponectin receptor 1 (AdipoR1), which was necessary for subsequent activation of Ca^{2+}/calmodulin-dependent protein kinase kinase β (CaMKKβ), AMPK and SIRT1, increased expression and decreased acetylation of peroxisome proliferator-activated receptor γ coactivator-1α (PGC-1α), and increased mitochondria in myocytes. Moreover, muscle-specific disruption of AdipoR1 suppressed the adiponectin-mediated increase in intracellular Ca^{2+} concentration, and decreased the activation of CaMKK, AMPK and SIRT1 by adiponectin. Suppression of AdipoR1 also resulted in decreased PGC-1α expression and deacetylation, decreased mitochondrial content and enzymes, decreased oxidative type I myofibres, and decreased oxidative stress-detoxifying enzymes in skeletal muscle, which were associated with insulin resistance and decreased exercise endurance. Decreased levels of adiponectin and AdipoR1 in obesity may have causal roles in mitochondrial dysfunction and insulin resistance seen in diabetes.

Adiponectin (encoded by *Adipoq*)[1–4] is an anti-diabetic and anti-atherogenic adipokine. Plasma adiponectin levels are decreased in obesity, insulin resistance, and type 2 diabetes[5]. Administration of adiponectin has been shown to cause glucose-lowering effects and ameliorate insulin resistance in mice[6–8]. Conversely, adiponectin-deficient mice exhibit insulin resistance and diabetes[9,10]. This insulin-sensitizing effect of adiponectin seems to be mediated by an increase in fatty acid oxidation by activation of AMP-activated protein kinase (AMPK)[11–13] and also by peroxisome proliferator-activated receptor α (PPARα)[14,15].

We previously reported the cloning of complementary DNAs encoding adiponectin receptors 1 and 2 (*Adipor1* and *Adipor2*) by expression cloning[16]. AdipoR1 is abundantly expressed in skeletal muscle and liver, whereas AdipoR2 is predominantly expressed in the liver. Both receptors are predicted to contain seven-transmembrane domains[16], but to be structurally and functionally distinct from G-protein-coupled receptors[17–19]. Adiponectin receptors may thus be thought to comprise a new receptor family.

We previously showed using *Adipor1* and/or *Adipor2* knockout mice that AdipoR1 and AdipoR2 act as the major receptors for adiponectin *in vivo*, and have important roles in the regulation of glucose and lipid metabolism, inflammation and oxidative stress *in vivo*[20]. Moreover, in the liver, AdipoR1 activated AMPK pathways and AdipoR2 activated PPARα pathways[20]. Therefore, identification of the 'missing link' between adiponectin receptors and adiponectin-activated key molecules is an important next step towards our understanding of the actions of adiponectin.

Insulin resistance has been reported to be associated with mitochondrial dysfunction[21]. However, the exact cause of mitochondrial dysfunction has yet to be ascertained. To clarify whether decreased adiponectin/AdipoR1 signalling could be associated with mitochondrial dysfunction, we analysed muscle-specific *Adipor1*-knockout (muscle-R1KO) mice, and attempted to determine the signalling mechanisms by which adiponectin/AdipoR1 would exert their biological effects.

Decreased PGC-1α and mitochondria in muscle-R1KO

Muscle-R1KO mice showed decreased phosphorylation of AMPK (Fig. 1a). Moreover, the administration of adiponectin increased the phosphorylation of AMPK in the muscle of control littermates but not in those of muscle-R1KO mice (Supplementary Fig. 1a), whereas adiponectin increased the phosphorylation of AMPK in the liver of both genotypes (Supplementary Fig. 1b). Muscle-R1KO mice also exhibited decreased molecules involved in mitochondrial biogenesis, such as PGC-1α[22], at both messenger RNA (*Ppargc1a*) (Fig. 1b) and protein levels (Fig. 1c). Adiponectin increased the expression levels of *Ppargc1a* in muscles of control littermates but not in those of muscle-R1KO mice (Supplementary Fig. 1c).

Muscle-R1KO mice showed decreases in molecules involved in mitochondrial biogenesis such as oestrogen-related receptor α (*Esrra*)[23], molecules involved in transcription such as nuclear respiratory factor 1 (*Nrf1*), and molecules involved in mitochondrial DNA replication/translation such as mitochondrial transcription factor A (*Tfam*)

[1]Department of Diabetes and Metabolic Diseases, Graduate School of Medicine, [2]Department of Integrated Molecular Science on Metabolic Diseases, 22nd Century Medical and Research Center, [3]Department of Neurobiology, Graduate School of Medicine, [4]Department of Pathology, Graduate School of Medicine, [5]Department of Biochemistry and Molecular Biology, Faculty of Medicine, The University of Tokyo, Tokyo 113-0033, Japan. [6]Department of Applied Biological Chemistry, Graduate School of Agricultural and Life Sciences, The University of Tokyo, Tokyo 113-8657, Japan. [7]Department of Integrated Biosciences, The University of Tokyo, Chiba 277-8562, Japan. [8]Department of Molecular Genetics, Graduate School of Medical Sciences, Kumamoto University, Kumamoto 860-0811, Japan. [9]Graduate School of Comprehensive Human Sciences, University of Tsukuba, Tsukuba 305-8577, Japan. [10]Department of Neuromuscular Research, National Institute of Neuroscience, National Center of Neurology and Psychiatry, Kodaira, Tokyo 187-8502, Japan.
*These authors contributed equally to this work.

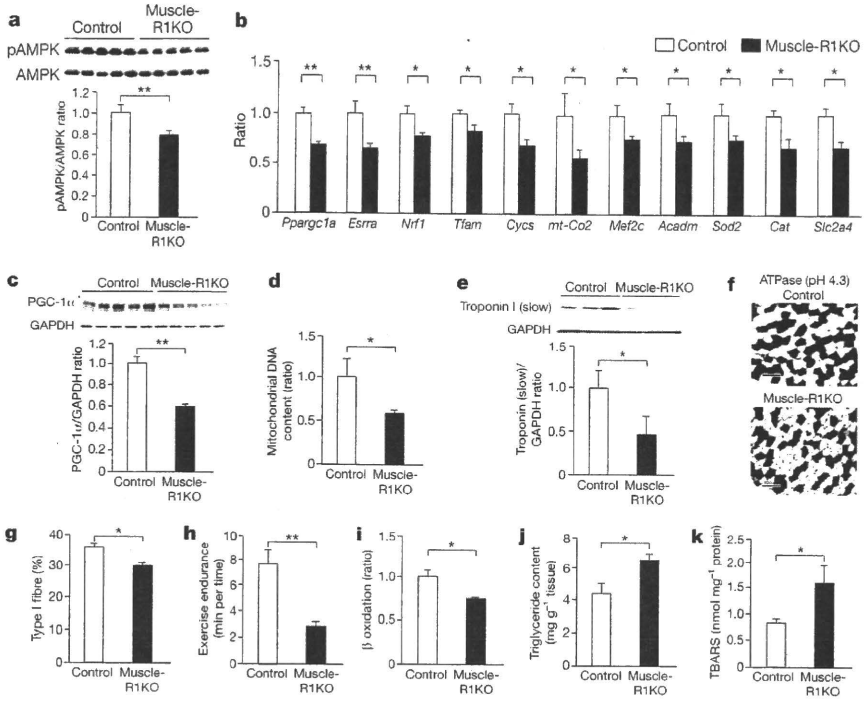

Figure 1 | Decreased mitochondria, oxidative type I myofibres and exercise capacity in skeletal muscle of muscle-R1KO mice. **a–k**, Phosphorylation and amount of AMPK (**a**), *Ppargc1a*, *Esrra*, *Nrf1*, *Tfam*, *Cycs*, *mt-Co2*, *Mef2c*, *Acadm*, *Sod2*, *Cat* and *Slc2a4* mRNA levels (**b**), PGC-1α protein levels (**c**), mitochondrial content as assessed by mitochondrial DNA copy number (**d**), amounts of troponin I (slow) protein (**e**), ATPase (pH 4.3 for type I fibres) staining of soleus muscles (scale bars, 100 μm) (**f**), quantification of type I fibres (**g**) based on fibre-type analyses (**f**), exercise endurance (**h**), β oxidation (**i**), triglyceride content (**j**), and TBARS (**k**) in skeletal muscle (**a–g**, **i–k**) obtained from control or muscle-R1KO after 5 h fasting. All values are presented as mean ± s.e.m. $n = 5$–12, $^{*}P < 0.05$ and $^{**}P < 0.01$ compared to control mice.

(Fig. 1b). Moreover, the expression levels of several oxidative phosphorylation and other mitochondrial genes were significantly reduced in muscle-R1KO mice, including cytochrome *c* (*Cycs*), and cytochrome *c* oxidase subunit II (*mt-Co2*) (Fig. 1b). Furthermore, muscle-R1KO mice had a decreased mitochondrial DNA content (Fig. 1d).

Mitochondrial function was assessed by measuring the enzymatic activities of Cox (Supplementary Fig. 2a) and succinate dehydrogenase (SDH) (Supplementary Fig. 2b). Staining of soleus muscle sections revealed a lower number of Cox- and SDH-positive muscle fibres and a decreased intensity of Cox and SDH staining in muscle-R1KO mice (Supplementary Fig. 2a, b).

Decreased type I fibres and exercise capacity in muscle-R1KO

Muscle-R1KO mice had decreased molecules involved in type I fibre[24] differentiation myocyte enhancer factor 2C (*Mef2c*)[25] (Fig. 1b) as well as the type I fibre marker troponin I (slow) (Fig. 1e). In contrast, muscle-R1KO mice had almost the same expression levels of MHCIIa, MHCIIx and MHCIIb as those seen in control mice (Supplementary Fig. 2c–e), indicating a reduction in oxidative, high endurance fibres in muscle-R1KO mice. These findings were consistent with the histological analysis performed (Fig. 1f, g). In soleus muscle of muscle-R1KO mice, type I fibres were reduced by 20% (Fig. 1g).

To study the effect of *Adipor1* ablation on skeletal muscle function in intact animals, we challenged control and muscle-R1KO mice with involuntary physical-exercise-assessed muscle endurance by treadmill running. Muscle endurance was significantly lower for muscle-R1KO mice than control mice (Fig. 1h).

We next examined the expression of metabolic genes and found that molecules involved in fatty-acid oxidation, such as medium-chain acyl-CoA dehydrogenase (*Acadm*), were significantly decreased in muscle-R1KO mice (Fig. 1b), which was associated with decreased β oxidation (Fig. 1i) and increased triglyceride content (Fig. 1j) in skeletal muscle.

Muscle-R1KO mice exhibited decreased expression levels of mitochondrial and cytoplasmic oxidative-stress-detoxifying genes such as manganese superoxide dismutase (*Sod2*) (Fig. 1b) and catalase (*Cat*) (Fig. 1b), respectively, and increased oxidative stress such as thiobarbituric acid reactive substance (TBARS) (Fig. 1k) in muscle. Expression of the insulin-sensitive glucose transporter 4 (*Slc2a4*) was reduced in muscle-R1KO mice (Fig. 1b).

Insulin resistance in muscle-R1KO mice

Plasma glucose and insulin levels after glucose administration were significantly higher in muscle-R1KO mice than in control mice (Fig. 2a, b). The capacities of muscle-R1KO mice to regulate plasma glucose levels after a bolus of insulin were significantly decreased as compared with control mice (Fig. 2c).

We performed a hyperinsulinaemic-euglycaemic clamp experiment. Disruption of *Adipor1* in muscle did not significantly alter endogenous glucose production, whereas it significantly decreased the glucose disposal rate and the glucose infusion rate, indicating decreased insulin sensitivity in muscle (Fig. 2d–f).

In agreement with the data obtained from the hyperinsulinaemic-euglycaemic clamps, decreased tyrosine phosphorylation of IRS-1 (Fig. 2g) and decreased phosphorylation of Ser 473 in Akt (Fig. 2h) stimulated with insulin in skeletal muscle of muscle-R1KO mice were found, which seemed to be associated with increased phosphorylation of S6K1 (Fig. 2i) and JNK (Fig. 2j). Ser 302 in mice IRS-1 has been reported to be phosphorylated by JNK[26], and the phosphorylation of Ser 636/639 has been reported to be mediated by mTOR and S6K1 pathways[27], both of which would result in inhibition of insulin signalling. The amounts of Ser 302 and Ser 636/639 phosphorylation in IRS-1 were increased in skeletal muscle of muscle-R1KO mice (Fig. 2k, l).

CaMKKβ is required for adiponectin/AdipoR1-induced PGC-1α

We next investigated the molecular mechanisms by which muscle-R1KO mice exhibited these phenotypes described earlier. Incubation of C2C12 myocytes with 30 μg ml^{-1} adiponectin increased mitochondrial DNA content (Fig. 3a). AMPK activity is dependent on the phosphorylation of AMPKα(Thr 172) in its activation loop by AMPK kinases (AMPKKs)[13,28]. LKB1 and CaMKKβ are known to be two major AMPKKs present in a variety of tissues and cells[13,29,30]. Suppression of AdipoR1 or CaMKKβ, or both AMPKα1 and AMPKα2 or PGC-1α expression by each specific short interfering RNA (siRNA) (Supplementary Fig. 3a–e) markedly reduced the increases in mitochondrial DNA content induced by adiponectin (Fig. 3a). In contrast, the suppression of AdipoR2 expression by

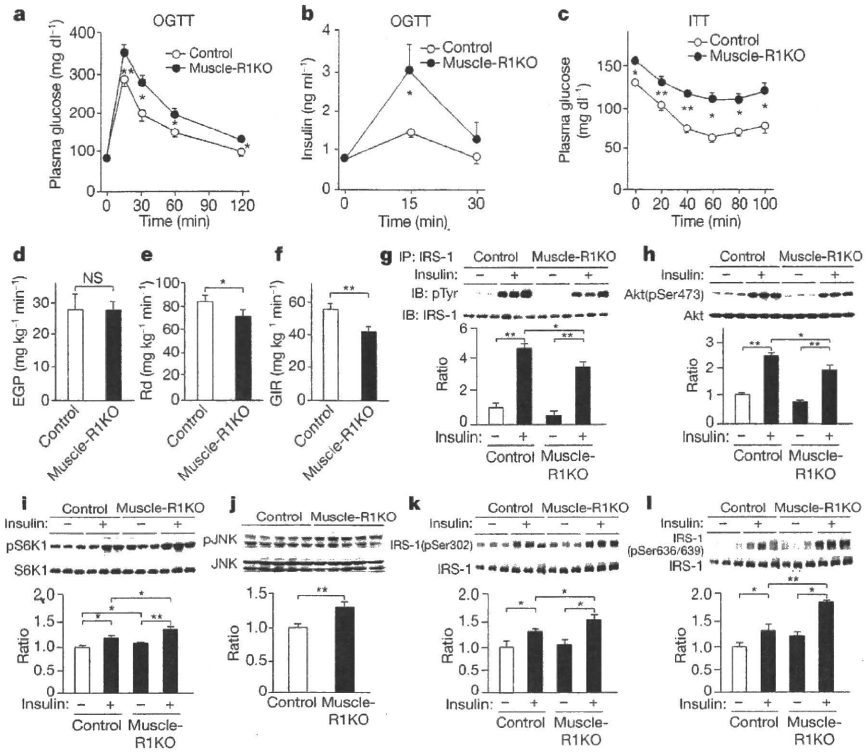

Figure 2 | Mechanisms of abnormal glucose and insulin homeostasis in muscle-R1KO mice. **a–f**, Plasma glucose (**a**, **c**) and plasma insulin (**b**) during an oral glucose tolerance test (OGTT) (1.5 g glucose per kg body weight) (**a**, **b**) or during an insulin tolerance test (ITT) (0.25 U insulin per kg body weight) (**c**), endogenous glucose production (EGP) (**d**), rates of glucose disposal (Rd) (**e**) and glucose infusion rate (GIR) (**f**) during a hyperinsulinaemic-euglycaemic clamp study in control and muscle-R1KO mice. **g–l**, Phosphorylation of tyrosine (pTyr) (**g**), Ser 302 (**k**) and Ser 636/639 (**l**) in IRS-1, phosphorylation and amount of Akt (**h**), S6K1 (**i**) and JNK (**j**) in skeletal muscle treated with or without insulin (0.3 U per kg body weight) for 7.5 min in control and muscle-R1KO mice after 5 h fasting. IB, immunoblot; IP, immunoprecipitate. All values are presented as mean ± s.e.m. $n = 6$–15 from 3–5 independent experiments, $^*P < 0.05$ and $^{**}P < 0.01$ compared to control or as indicated. NS, not significant.

specific siRNA (Supplementary Fig. 3f) failed to significantly reduce mitochondrial biogenesis induced by adiponectin (Fig. 3a).

Suppression of AdipoR1 or CaMKKβ expression by each specific siRNA (Supplementary Fig. 3a, b) greatly reduced the increase in PGC-1α expression induced by adiponectin (Fig. 3b). Interestingly, the suppression of AMPKα1 and AMPKα2 expression by each specific siRNA (Supplementary Fig. 3c, d) failed to significantly reduce PGC-1α expression induced by adiponectin (Fig. 3b), suggesting that PGC-1α expression was induced by adiponectin via an AdipoR1- and CaMKKβ-dependent yet AMPK-independent pathway.

PGC-1α has been reported to be activated by AMPK via phosphorylation[31] and by deacetylation through SIRT1 activation[32]. We next addressed the possibility that AMPK activated by adiponectin and AdipoR1 could regulate PGC-1α activities. Treatment of C2C12 myocytes with adiponectin decreased PGC-1α acetylation after 2 h of treatment (Fig. 3c). Suppression of AdipoR1 or both AMPKα1 and AMPKα2 or SIRT1 expression by each specific siRNA (Supplementary Fig. 3a, c, d, g) largely abrogated the decrease in PGC-1α acetylation induced by adiponectin (Fig. 3c). The PGC-1α-2A mutant lacking the two AMPK phosphorylation sites[31] showed markedly reduced PGC-1α deacetylation and mitochondrial biogenesis with adiponectin (Fig. 3d, e).

Adiponectin failed to induce mitochondrial biogenesis further in the C2C12 myocytes expressing PGC-1α-R13 in which 13 of the potential lysine acetylation sites were mutated into arginine[32] (Fig. 3f). Because the capacity for undergoing acetylation is impaired in the PGC-1α-R13 mutant, these data are consistent with the dependence of adiponectin on SIRT1-mediated deacetylation of PGC-1α in activating PGC-1α.

SIRT1 deacetylase activity has been reported to be driven by NAD^+ levels[32,33]. Adiponectin increased the NAD^+/NADH ratio in C2C12 myocytes (Fig. 3g). Muscle-R1KO mice also showed increased PGC-1α acetylation (Fig. 3h) and decreased the NAD^+/NADH ratio stimulated with adiponectin (Fig. 3i) *in vivo*. These data indicated that the total activity as assessed by multiplying expression and deacetylation of PGC-1α is markedly reduced in muscle-R1KO mice (Supplementary Fig. 4).

Adiponectin induces Ca^{2+} influx by AdipoR1

Interestingly, treatment of C2C12 myocytes with adiponectin resulted in an increase in the intracellular Ca^{2+} concentration measured by fura-2-based fluorescent imaging (Fig. 4a). C2C12 myocytes showed responses to adiponectin in a dose-dependent manner (data not shown). Removal of extracellular free Ca^{2+} by EGTA almost completely abolished the adiponectin-induced Ca^{2+} response (Fig. 4a), whereas EGTA had no effect on the ATP-induced intracellular Ca^{2+} release (data not shown). Suppression of AdipoR1 expression using a specific siRNA (Fig. 4b) largely reduced the calcium response of C2C12 myocytes to adiponectin (Fig. 4c, d). These results indicate that the influx of extracellular Ca^{2+} after adiponectin treatment of C2C12 myocytes is mediated by AdipoR1.

To study further the importance of AdipoR1 for adiponectin-induced Ca^{2+} response in the gain-of-function experiments, we expressed AdipoR1 in *Xenopus laevis* oocytes (Fig. 4e). The increase in intracellular calcium levels stimulated with adiponectin was detected by monitoring Ca^{2+}-activated Cl^- currents in AdipoR1 complementary-RNA-injected oocytes (Fig. 4f, g). The responses were not observed in control oocytes (Fig. 4g). We studied the effect of removal of extracellular free Ca^{2+} by EGTA on the Ca^{2+}-activated Cl^- current response to adiponectin of *Xenopus* oocytes expressing AdipoR1. We found that the removal of extracellular free Ca^{2+} by EGTA almost completely abolished the Ca^{2+}-activated Cl^- current response to adiponectin of *Xenopus* oocytes expressing AdipoR1 (Fig. 4g), indicating that these responses were dependent on extracellular Ca^{2+}.

Adiponectin-induced Ca^{2+} influx is important for its actions

Incubation of C2C12 myocytes with adiponectin increased the phosphorylation of the AMPK α-subunit at Thr 172, and EGTA partially suppressed adiponectin-induced increased AMPK phosphorylation (Fig. 5a). As expected, EGTA almost completely abolished ionomycin-dependent phosphorylation of AMPK, whereas EGTA had no effect on 5-aminoimidazole-4-carboxamide-1-β-D-riboside (AICAR)-induced phosphorylation of AMPK in C2C12 myocytes (Fig. 5a).

Suppression of CaMKKβ or LKB1 expression by each specific siRNA (Supplementary Fig. 3b, h) significantly reduced the increases in

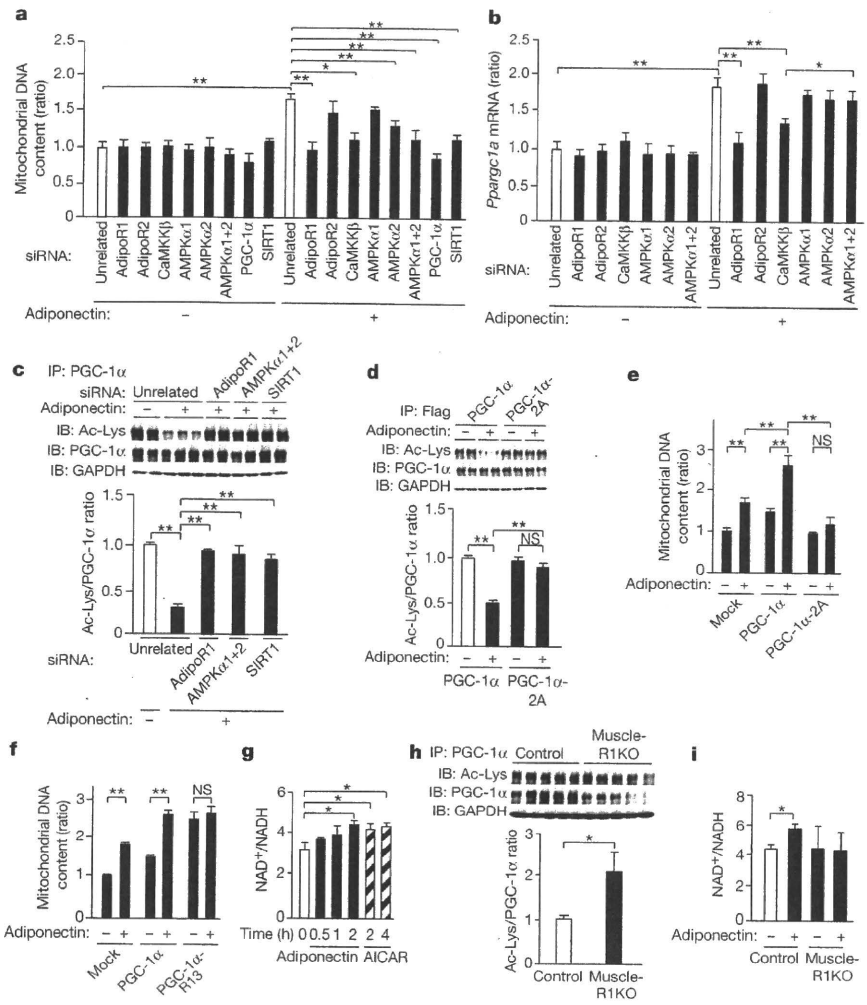

Figure 3 | Adiponectin/AdipoR1 increase PGC-1α expression and activity, and mitochondrial biogenesis in C2C12 myocytes. **a–i**, Mitochondrial content as assessed by mitochondrial DNA copy number (**a**, **e**, **f**), *Ppargc1a* mRNA levels (**b**), acetyl-lysine (Ac-Lys) levels checked on PGC-1α or Flag immunoprecipitates (**c**, **d**, **h**), NAD^+/NADH ratio (**g**, **i**) in C2C12 myocytes treated with adiponectin for the times indicated (**g**), in C2C12 myocytes transfected with the indicated siRNA duplex (**a–c**), in C2C12 myocytes transfected with the wild-type or the 2A mutant form of PGC-1α (**d**, **e**) or the R13 mutant form of PGC-1α (**f**) treated with 10 μg ml^{-1} adiponectin for 48 h (**a**, **e**, **f**) or for 1.5 h (**b**) or 2 h (**c**, **d**), or in skeletal muscle from control or muscle-R1KO mice treated with or without adiponectin (**h**, **i**). The supernatant was blotted against GAPDH as an input control (**c**, **d**, **h**). C2C12 myocytes were used after myogenic differentiation in all experiments. All values are presented as mean ± s.e.m. $n = 5–10$, $^*P < 0.05$ and $^{**}P < 0.01$ compared to control or unrelated siRNA or as indicated.

phosphorylation of AMPK induced by adiponectin (Fig. 5b). Although the AMPK inhibitor AraA only tended to reduce adiponectin-induced PGC-1α expression, Ca^{2+} removal by EGTA or inhibition of CaMKKβ with its selective inhibitor STO-609 (ref. 34) effectively and almost completely abolished increased PGC-1α expression stimulated with adiponectin in C2C12 myocytes (Fig. 5c), as removal of extracellular Ca^{2+} effectively abolishes the Ca^{2+} signal evoked by adiponectin (Fig. 4a).

Finally, we examined whether adiponectin-induced Ca^{2+} influxes into skeletal muscle might be impaired in muscle-R1KO mice through *in vivo* imaging[35,36]. We found that whereas treatment of soleus muscle with adiponectin resulted in an increase in the intracellular Ca^{2+} concentration as measured by fura-2-based fluorescent imaging in control mice, muscle-R1KO mice almost completely abrogated the calcium response of soleus muscle to adiponectin (Fig. 5d–f), consistent with the observation that adiponectin significantly increased the phosphorylation of CaMKI[37,38], an intracellular substrate of CaMKKβ, by AdipoR1 in skeletal muscle *in vivo* (Supplementary Fig. 5).

We also attempted to examine whether simultaneous activation of Ca^{2+} signalling and AMPK/SIRT1 pathways by exercise, independent of AdipoR1, could rescue phenotype in muscle-R1KO mice. Two weeks of exercise significantly ameliorated insulin resistance, and increased mitochondrial content and function such as citrate synthase activities in muscles of muscle-R1KO mice (Fig. 6a–d).

Discussion

Here we provide evidence that muscle-R1KO mice exhibit decreased mitochondrial content and enzymes. PGC-1α is a key regulator of mitochondrial content and function. Expression of PGC-1α has been reported to be modulated in several physiological contexts, for example, in skeletal muscle in response to exercise partly by increased Ca^{2+} signalling via molecules such as CaMK and CREB[39]. Activities of PGC-1α have also been reported to be modulated by several kinds of PGC-1α modifications, such as phosphorylation by AMPK[31] and deacetylation by AMPK and SIRT1[32]. AMPK and SIRT1 could also be activated by exercise. We have demonstrated that muscle-R1KO mice exhibit decreased PGC-1α expression as well as decreased deacetylation of PGC-1α. Consistent with this, adiponectin induced Ca^{2+} influx by AdipoR1, thereby activating CaMKKβ, which led to increased PGC-1α expression. Moreover, adiponectin/AdipoR1 activated AMPK and SIRT1, thereby inducing PGC-1α deacetylation. These data indicated that adiponectin and AdipoR1 stimulate increases in both the expression and activation of PGC-1α, in a similar fashion to exercise (Fig. 6e).

Although the degree of decreased PGC-1α expression was approximately 40% in muscle-R1KO mice, the extent of decreased mitochondrial biogenesis and decreased exercise endurance were comparable to those observed in muscle-specific PGC-1α-knockout mice[40], which may be explained by the finding that adiponectin and AdipoR1 increase not only PGC-1α expression but also PGC-1α activity (Fig. 6e).

Importantly, decreases in the expression of AdipoR1 and PGC-1α and mitochondrial DNA content were also observed in type 2 diabetic patients[41] and individuals at increased risk of developing diabetes owing to their family history[42], as well as in obese diabetic *db/db* mice (Supplementary Fig. 6a–c). These data indicate that decreased

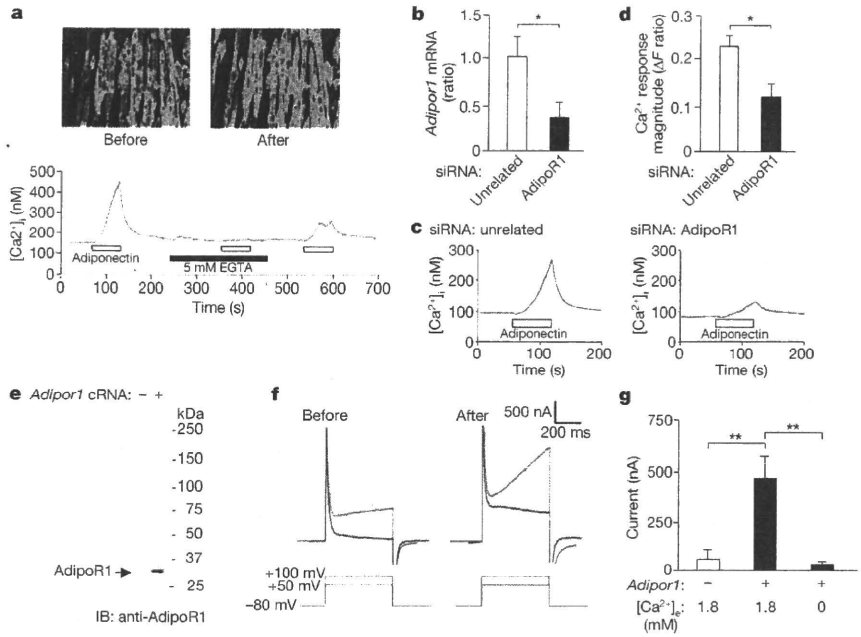

Figure 4 | Adiponectin-induced Ca^{2+} influx by AdipoR1 in C2C12 myocytes and *Xenopus* oocytes. **a**, Pseudocoloured images of changes in fura-2 before and after 1 min stimulation with adiponectin (30 μg ml^{-1}). Red corresponds to the greatest response. The bottom trace demonstrates the average calcium response of C2C12 myocytes to 1-min stimulation with adiponectin along with application of 5 mM EGTA (black bar). The shaded region around the trace represents s.e.m. **b–d**, *Adipor1* mRNA levels (**b**), fura-2 calcium response (**c**) and their magnitude (**d**) of C2C12 myocytes transfected with unrelated siRNA duplex or AdipoR1 siRNA duplex to stimulation with 30 μg ml^{-1} adiponectin for 1 min. **e–g**, The amounts of AdipoR1 protein (**e**), representative Ca^{2+}-activated Cl^- current traces (**f**) before (left) and after (right) 30-s application of adiponectin, and their magnitude (**g**) in *Xenopus* oocytes injected with or without *Adipor1* cRNA in response to adiponectin (30 μg ml^{-1}), and with or without application of 5 mM EGTA with depolarizing pulses of +100 mV. $[Ca^{2+}]_i$ and $[Ca^{2+}]_e$, intracellular and external Ca^{2+} concentration, respectively. All values are presented as mean ± s.e.m. $n = 6–14$, $^*P < 0.05$ and $^{**}P < 0.01$ compared to unrelated siRNA cells or control cells or as indicated.

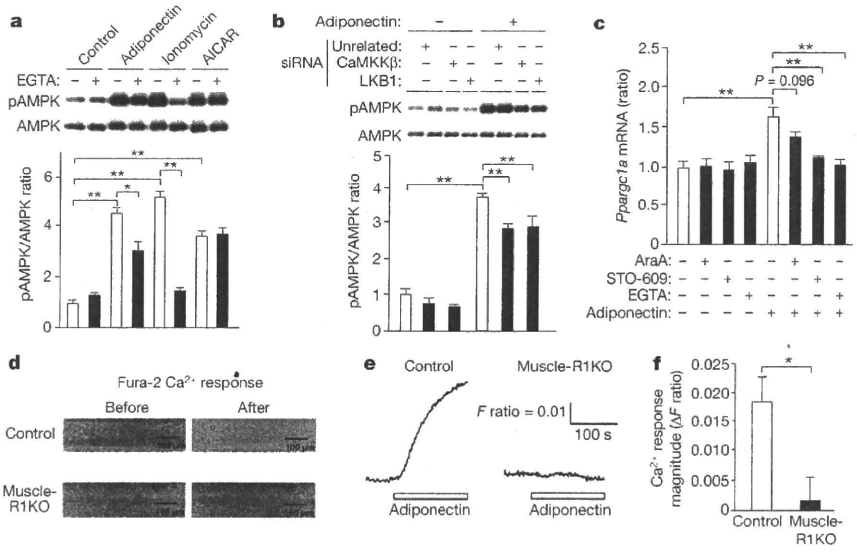

Figure 5 | Adiponectin-induced Ca^{2+} influx is required for CaMKK and AMPK activation and PGC-1α expression. **a**, **b**, Phosphorylation and amount of AMPK in C2C12 myocytes preincubated for 20 min with or without 5 mM EGTA and then treated for 5 min with adiponectin (30 μg ml^{-1}) or ionomycin (1 μM), or for 1 h with AICAR (1 mM) (**a**), or C2C12 myocytes transfected with the indicated siRNA duplex and then treated with 30 μg ml^{-1} adiponectin for 5 min (**b**). **c**, Amount of *Ppargc1a* mRNA in C2C12 myocytes preincubated for 1 h with AraA (0.5 mM) or for 6 h with STO-609 (1 μg ml^{-1}) or for 20 min with EGTA (5 mM), and then treated for 1.5 h with or without adiponectin (10 μg ml^{-1}). **d**, Representative pseudocoloured images of changes in the fura-2 calcium response before and after 5 min stimulation with adiponectin (30 μg ml^{-1}) in a soleus muscle from control mice (top) and muscle-R1KO mice (bottom). Red corresponds to the greatest response. Scale bars, 100 μm. **e**, Trace demonstrates the calcium response of soleus muscle in the fields presented in **d**. Adiponectin was applied during the indicated period. **f**, The magnitude of fura-2 calcium response signals by 160-s adiponectin stimulation to soleus muscles. ΔF ratio indicates the change in the fluorescence ratio after adiponectin application. All values are presented as mean ± s.e.m. $n = 5–10$, $^*P < 0.05$ and $^{**}P < 0.01$ compared to control or unrelated siRNA cells or as indicated.

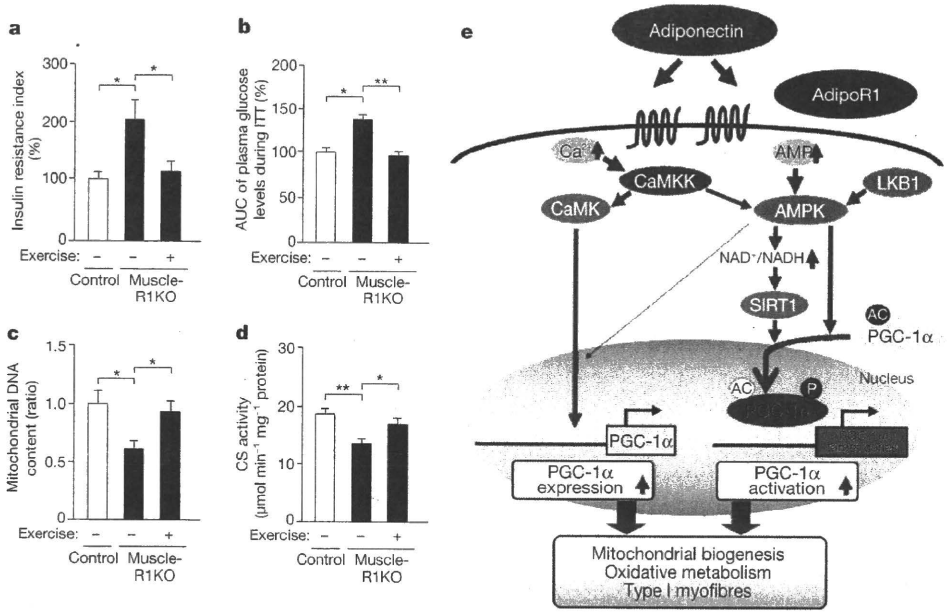

Figure 6 | The effect of exercise on muscle-R1KO mice. a–d, The insulin resistance index (**a**), area under the curves (AUC) of plasma glucose levels during the ITT (**b**), mitochondrial content as assessed by mitochondrial DNA copy number (**c**), and citrate synthase (CS) enzyme activity (**d**) in skeletal muscle of control and muscle-R1KO mice after 2 weeks exercise. The results are expressed as the percentage of the value in control littermates (**a**, **b**). **e,** Scheme illustrating the signal transduction of adiponectin/AdipoR1 in muscle cells. Both CaMKKβ and LKB1 are necessary for adiponectin-induced full AMPK activation. AMPK and SIRT1 are required for adiponectin/AdipoR1-induced PGC-1α activation. CaMKKβ activation by adiponectin-induced Ca^{2+} influx via AdipoR1 is required for adiponectin-induced increased PGC-1α expression. PGC-1α is required for mitochondrial biogenesis stimulated with adiponectin/AdipoR1. From these data, we conclude that adiponectin and AdipoR1 increase PGC-1α expression and activity by Ca^{2+} signalling and by AMPK and SIRT1, leading to increased mitochondrial biogenesis. We focused on the molecules that we have obtained direct evidence by both gain-of-function and loss-of-function experiments *in vitro* and *in vivo*, except for CaMK, which has already been reported to increase PGC-1α expression by other researchers[39]. AC, acetylation. All values are presented as mean ± s.e.m. $n = 5–8$, $*P < 0.05$ and $**P < 0.01$ compared to control mice or as indicated.

adiponectin/AdipoR1 in pathophysiological conditions such as obesity may have causal roles in the development of PGC-1α dysregulation and mitochondrial dysfunction.

In skeletal muscle AdipoR1 regulated insulin sensitivity by several mechanisms (Supplementary Fig. 7). First is the activation of S6K1, which has been reported to be able to cause insulin resistance by increased phosphorylation of Ser 636/639 in IRS-1 (ref. 27). S6K1 is crucially inhibited by AMPK[43]. In skeletal muscle of muscle-R1KO mice, AMPK activation was reduced, whereas activation of S6K1 and phosphorylation of Ser 636/639 in IRS-1 were indeed increased. Second is the increased oxidative stress, which has been causally linked to insulin resistance[44] by increased phosphorylation of Ser 302 in IRS-1 through JNK activation[26]. Several oxidative stress detoxification genes are crucially regulated by AMPK and PGC-1α[45], and the expression levels of these genes such as *Sod2* and *Cat* were reduced, which was associated with increased TBARS in skeletal muscle of muscle-R1KO mice. Third is the increased triglyceride content, which has been associated with insulin resistance by increased phosphorylation of Ser 302 in IRS-1 through JNK activation[26]. Molecules involved in fatty-acid oxidation are crucially regulated by AMPK and PGC-1α, and the expression levels of these genes such as *Mcad* were reduced, which was associated with increased triglyceride content in skeletal muscle of muscle-R1KO mice. Consistent with increased TBARS and triglyceride content, JNK activation and phosphorylation of Ser 302 in IRS-1 were indeed increased.

Exercise has been reported to have beneficial effects on longevity and lifestyle-related diseases, and at the same time to activate Ca^{2+}, AMPK, SIRT1 and PGC-1α pathways[39]. In this study, we clearly demonstrated that adiponectin and AdipoR1 regulate PGC-1α and mitochondria via Ca^{2+} and AMPK/SIRT1. Therefore, agonism of AdipoR1 as well as strategies to increase AdipoR1 in muscle could be exercise-mimetics.

In conclusion, AdipoR1 has a crucial role in the physiological and pathophysiological significance of adiponectin in muscle, and is involved in the regulation of Ca^{2+} signalling, PGC-1α expression and activation, mitochondrial function and oxidative stress, glucose and lipid metabolism, and exercise endurance. This study suggests that agonism of AdipoR1, as well as strategies to increase AdipoR1 in muscle, may be logical approaches to providing a new treatment modality for mitochondrial dysfunction, insulin resistance and type 2 diabetes linked to obesity.

METHODS SUMMARY

Mice. Mice were 8–10 weeks of age at the time of the experiment. The animal care and use procedures were approved by the Animal Care Committee of the University of Tokyo.

Measurement of exercise capacity in muscle-R1KO mice. The treadmill exercise test regimen was 15 m min^{-1} for 20 min. Exercise endurance was assessed by dividing 20 min by the number of times a mouse was unable to avoid electrical shocks.

Studies with C2C12 cells. Induction of myogenic differentiation was carried out according to a method described previously[41]. By day 5, the cells had differentiated into multinucleated contracting myocytes. C2C12 myocytes were used after myogenic differentiation in all experiments.

Plasmids. The plasmids encoding PGC-1α and the PGC-1α-2A mutant were generous gifts from B. M. Spiegelman, and have all been described previously[31]. The plasmids encoding for the PGC-1α-R13 mutant were generous gifts from P. Puigserver, and have all been described previously[32].

Statistical analysis. Results are expressed as mean ± s.e.m. Differences between two groups were assessed using unpaired two-tailed *t*-tests. Data involving more than two groups were assessed by analysis of variance (ANOVA).

Received 12 August 2009; accepted 11 March 2010.
Published online 31 March 2010.

1. Scherer, P. E., Williams, S., Fogliano, M., Baldini, G. & Lodish, H. F. A novel serum protein similar to C1q, produced exclusively in adipocytes. *J. Biol. Chem.* 270, 26746–26749 (1995).

2. Hu, E., Liang, P. & Spiegelman, B. M. AdipoQ is a novel adipose-specific gene dysregulated in obesity. *J. Biol. Chem.* **271**, 10697–10703 (1996).
3. Maeda, K. *et al.* cDNA cloning and expression of a novel adipose specific collagen-like factor, apM1 (AdiPose Most abundant Gene transcript 1). *Biochem. Biophys. Res. Commun.* **221**, 286–289 (1996).
4. Nakano, Y., Tobe, T., Choi-Miura, N.-H., Mazda, T. & Tomita, M. Isolation and characterization of GBP28, a novel gelatin-binding protein purified from human plasma. *J. Biochem.* **120**, 803–812 (1996).
5. Hotta, K. *et al.* Plasma concentrations of a novel, adipose-specific protein, adiponectin, in type 2 diabetic patients. *Arterioscler. Thromb. Vasc. Biol.* **20**, 1595–1599 (2000).
6. Fruebis, J. *et al.* Proteolytic cleavage product of 30-kDa adipocyte complement-related protein increases fatty acid oxidation in muscle and causes weight loss in mice. *Proc. Natl Acad. Sci. USA* **98**, 2005–2010 (2001).
7. Yamauchi, T. *et al.* The fat-derived hormone adiponectin reverses insulin resistance associated with both lipoatrophy and obesity. *Nature Med.* **7**, 941–946 (2001).
8. Berg, A. H., Combs, T. P., Du, X., Brownlee, M. & Scherer, P. E. The adipocyte-secreted protein Acrp30 enhances hepatic insulin action. *Nature Med.* **7**, 947–953 (2001).
9. Kubota, N. *et al.* Disruption of adiponectin causes insulin resistance and neointimal formation. *J. Biol. Chem.* **277**, 25863–25866 (2002).
10. Maeda, N. *et al.* Diet-induced insulin resistance in mice lacking adiponectin/ACRP30. *Nature Med.* **8**, 731–737 (2002).
11. Yamauchi, T. *et al.* Adiponectin stimulates glucose utilization and fatty-acid oxidation by activating AMP-activated protein kinase. *Nature Med.* **8**, 1288–1295 (2002).
12. Tomas, E. *et al.* Enhanced muscle fat oxidation and glucose transport by ACRP30 globular domain: acetyl-CoA carboxylase inhibition and AMP-activated protein kinase activation. *Proc. Natl Acad. Sci. USA* **99**, 16309–16313 (2002).
13. Kahn, B. B., Alquier, T., Carling, D. & Hardie, D. G. AMP-activated protein kinase: ancient energy gauge provides clues to modern understanding of metabolism. *Cell Metab.* **1**, 15–25 (2005).
14. Kersten, S., Desvergne, B. & Wahli, W. Roles of PPARs in health and disease. *Nature* **405**, 421–424 (2000).
15. Yamauchi, T. *et al.* Globular adiponectin protected ob/ob mice from diabetes and apoE deficient mice from atherosclerosis. *J. Biol. Chem.* **278**, 2461–2468 (2003).
16. Yamauchi, T. *et al.* Cloning of adiponectin receptors that mediate antidiabetic metabolic effects. *Nature* **423**, 762–769 (2003).
17. Wess, J. G-protein-coupled receptors: molecular mechanisms involved in receptor activation and selectivity of G-protein recognition. *FASEB J.* **11**, 346–354 (1997).
18. Yokomizo, T., Izumi, T., Chang, K., Takuwa, Y. & Shimizu, T. A. G-protein-coupled receptor for leukotriene B4 that mediates chemotaxis. *Nature* **387**, 620–624 (1997).
19. Scheer, A., Fanelli, F., Costa, T., De Benedetti, P. G. & Cotecchia, S. Constitutively active mutants of the α1B-adrenergic receptor: role of highly conserved polar amino acids in receptor activation. *EMBO J.* **15**, 3566–3578 (1996).
20. Yamauchi, T. *et al.* Targeted disruption of AdipoR1 and AdipoR2 causes abrogation of adiponectin binding and metabolic actions. *Nature Med.* **13**, 332–339 (2007).
21. Petersen, K. F. *et al.* Impaired mitochondrial activity in the insulin-resistant offspring of patients with type 2 diabetes. *N. Engl. J. Med.* **350**, 664–671 (2004).
22. Wu, Z. *et al.* Mechanisms controlling mitochondrial biogenesis and respiration through the thermogenic coactivator PGC-1. *Cell* **98**, 115–124 (1999).
23. Mootha, V. K. *et al.* Errα and Gabpa/b specify PGC-1α-dependent oxidative phosphorylation gene expression that is altered in diabetic muscle. *Proc. Natl Acad. Sci. USA* **101**, 6570–6575 (2004).
24. Berchtold, M. W. *et al.* Calcium ion in skeletal muscle: its crucial role for muscle function, plasticity, and disease. *Physiol. Rev.* **80**, 1215–1265 (2000).
25. Wu, H. *et al.* MEF2 responds to multiple calcium-regulated signals in the control of skeletal muscle fiber type. *EMBO J.* **19**, 1963–1973 (2000).
26. Hotamisligil, G. S. Inflammation and metabolic disorders. *Nature* **444**, 860–867 (2006).
27. Um, S. H. *et al.* Absence of S6K1 protects against age- and diet-induced obesity while enhancing insulin sensitivity. *Nature* **431**, 200–205 (2004).
28. Hawley, S. A. *et al.* Characterization of the AMP-activated protein kinase kinase from rat liver and identification of threonine 172 as the major site at which it phosphorylates AMP-activated protein kinase. *J. Biol. Chem.* **271**, 27879–27887 (1996).
29. Hawley, S. A. *et al.* Calmodulin-dependent protein kinase kinase-β is an alternative upstream kinase for AMP-activated protein kinase. *Cell Metab.* **2**, 9–19 (2005).
30. Woods, A. *et al.* Ca^{2+}/calmodulin-dependent protein kinase kinase-β acts upstream of AMP-activated protein kinase in mammalian cells. *Cell Metab.* **2**, 21–33 (2005).
31. Jäger, S., Handschin, C., St-Pierre, J. & Spiegelman, B. M. AMP-activated protein kinase (AMPK) action in skeletal muscle via direct phosphorylation of PGC-1α. *Proc. Natl Acad. Sci. USA* **104**, 12017–12022 (2007).
32. Rodgers, J. T. *et al.* Nutrient control of glucose homeostasis through a complex of PGC-1α and SIRT1. *Nature* **434**, 113–118 (2005).
33. Guarente, L. Sirtuins as potential targets for metabolic syndrome. *Nature* **444**, 868–874 (2006).
34. Tokumitsu, H. *et al.* STO-609, a specific inhibitor of the Ca^{2+}/calmodulin-dependent protein kinase kinase. *J. Biol. Chem.* **277**, 15813–15818 (2002).
35. Tóth, A. *et al.* Quantitative assessment of $[Ca^{2+}]_i$ levels in rat skeletal muscle *in vivo*. *Am. J. Physiol. Heart Circ. Physiol.* **275**, H1652–H1662 (1998).
36. Shkryl, V. M. & Shirokova, N. Transfer and tunneling of Ca^{2+} from sarcoplasmic reticulum to mitochondria in skeletal muscle. *J. Biol. Chem.* **281**, 1547–1554 (2006).
37. Anderson, K. A. *et al.* Components of a calmodulin-dependent protein kinase cascade. Molecular cloning, functional characterization and cellular localization of Ca^{2+}/calmodulin-dependent protein kinase kinase beta. *J. Biol. Chem.* **273**, 31880–31889 (1998).
38. Soderling, T. R. The Ca-calmodulin-dependent protein kinase cascade. *Trends Biochem. Sci.* **24**, 232–236 (1999).
39. Handschin, C. & Spiegelman, B. M. The role of exercise and PGC1α in inflammation and chronic disease. *Nature* **454**, 463–469 (2008).
40. Handschin, C. *et al.* Skeletal muscle fiber-type switching, exercise intolerance, and myopathy in PGC-1α muscle-specific knock-out animals. *J. Biol. Chem.* **282**, 30014–30021 (2007).
41. Mootha, V. K. *et al.* PGC-1α-responsive genes involved in oxidative phosphorylation are coordinately downregulated in human diabetes. *Nature Genet.* **34**, 267–273 (2003).
42. Patti, M. E. *et al.* Coordinated reduction of genes of oxidative metabolism in humans with insulin resistance and diabetes: Potential role of PGC1 and NRF1. *Proc. Natl Acad. Sci. USA* **100**, 8466–8471 (2003).
43. Wang, C. *et al.* Adiponectin sensitizes insulin signaling by reducing p70 S6 kinase-mediated serine phosphorylation of IRS-1. *J. Biol. Chem.* **282**, 7991–7996 (2007).
44. Houstis, N., Rosen, E. D. & Lander, E. S. Reactive oxygen species have a causal role in multiple forms of insulin resistance. *Nature* **440**, 944–948 (2006).
45. St-Pierre, J. *et al.* Suppression of reactive oxygen species and neurodegeneration by the PGC-1transcriptional coactivators. *Cell* **127**, 397–408 (2006).

Supplementary Information is linked to the online version of the paper at www.nature.com/nature.

Acknowledgements We thank B. M. Spiegelman for critical discussions and reading of the manuscript; T. Yokomizo for discussion and support; A. Tsuchida, K. Hara, Y. Hada, Y. Nio, T. Maki, T. Takazawa, Y. Iwata, M. Kobayashi, S. Kawamoto, K. Kobayashi, K. Hirota, Y. Shiomi, T. Mitsumatsu, L. Hirose, Y. Sea, M. Nakamura and K. Take for technical help and support; and S. Suzuki, K. Miyata, C. Ueda, A. Itoh and A. Okano for technical assistance. This work was supported by Grant-in-aid for Scientific Research (S) (20229008) (to T.K.), (B) (20390254) (to T.Y.), Targeted Proteins Research Program (to T.K.), the Global COE Research Program (to T.K.) and Translational Systems Biology and Medicine Initiative (to T.K.) from the Ministry of Education, Culture, Sports, Science and Technology of Japan.

Author Contributions M.I., M.O.-I., T.Y., K.S., T.N., M.F., M.Y., S.N., R.N., M.T., H.O., N.K., I.T., Y.K.H. and N.Y. performed experiments. T.K. and T.Y. conceived and supervised the study. K.T., T.S. and K.H. supervised the study. T.Y., T.K., M.I. and M.O-I. wrote the paper. All authors interpreted data.

Author Information Reprints and permissions information is available at www.nature.com/reprints. The authors declare no competing financial interests. Correspondence and requests for materials should be addressed to T.K. (kadowaki-3im@h.u-tokyo.ac.jp) or T.Y. (tyamau-tky@umin.net).

Cell Metabolism

Macrophage-Derived AIM Is Endocytosed into Adipocytes and Decreases Lipid Droplets via Inhibition of Fatty Acid Synthase Activity

Jun Kurokawa,[1] Satoko Arai,[1] Katsuhiko Nakashima,[1] Hiromichi Nagano,[1] Akemi Nishijima,[1] Keishi Miyata,[3] Rui Ose,[4] Mayumi Mori,[1] Naoto Kubota,[2] Takashi Kadowaki,[2] Yuichi Oike,[3] Hisashi Koga,[4] Maria Febbraio,[5] Toshihiko Iwanaga,[6] and Toru Miyazaki[1,*]

[1]Laboratory of Molecular Biomedicine for Pathogenesis, Center for Disease Biology and Integrative Medicine, Faculty of Medicine
[2]Department of Internal Medicine, Graduate School of Medicine
The University of Tokyo, Tokyo, 113-0033, Japan
[3]Department of Molecular Genetics, Graduate School of Medical Sciences, Kumamoto University, Kumamoto, 860-8556, Japan
[4]Department of Human Genome Research, Kazusa DNA Research Institute, Kisarazu, Chiba, 292-0818, Japan
[5]Department of Cell Biology, Lerner Research Institute, Cleveland Clinic Foundation, Cleveland, OH 44195, USA
[6]Department of Functional Morphology, Laboratory of Histology and Cytology, Hokkaido University Graduate School of Medicine, Sapporo, Hokkaido, 060-0815, Japan
*Correspondence: tm@m.u-tokyo.ac.jp
DOI 10.1016/j.cmet.2010.04.013

SUMMARY

Macrophages infiltrate adipose tissue in obesity and are involved in the induction of inflammation, thereby contributing to the development of obesity-associated metabolic disorders. Here, we show that the macrophage-derived soluble protein AIM is endocytosed into adipocytes via CD36. Within adipocytes, AIM associates with cytosolic fatty acid synthase (FAS), thereby decreasing FAS activity. This decreases lipid droplet size, stimulating the efflux of free fatty acids and glycerol from adipocytes. As an additional consequence of FAS inhibition, AIM prevents preadipocyte maturation. In vivo, the increase in adipocyte size and fat weight induced by high-fat diet (HFD) was accelerated in *AIM*-deficient ($AIM^{-/-}$) mice compared to $AIM^{+/+}$ mice. Moreover, injection of recombinant AIM in $AIM^{-/-}$ mice suppresses the increase in fat mass induced by HFD. Interestingly, metabolic rates are comparable in $AIM^{-/-}$ and $AIM^{+/+}$ mice, suggesting that AIM specifically influences adipocyte status. Thus, this AIM function in adipocytes may be physiologically relevant to obesity progression.

INTRODUCTION

It is well known that adipose tissues in obesity are in a state of chronic inflammation (Olshansky et al., 2005; Baker et al., 2007). Accumulating evidence indicates that this inflammation is induced predominantly by the recruitment of a large number of macrophages into adipose tissues (Olshansky et al., 2005; Baker et al., 2007; Apovian et al., 2008). Although the precise mechanism underlying the initiation of macrophage recruitment to adipose tissues remains a matter of debate, adipose tissue macrophage number rapidly increases as obesity progresses (Surmi and Hasty, 2008). The subclinical inflammatory state of adipose tissues is tightly associated with insulin resistance of adipose tissues as well as systemic insulin resistance and cardiovascular disease (Neels and Olefsky, 2006; Shoelson et al., 2006). Thus, adipose tissue macrophages are thought to play key roles in several obesity-induced metabolic disorders. However, whether adipose tissue macrophages also exert direct effect(s) on surrounding adipocytes, independent of inflammatory responses, remains to be determined. To address this question, we focused on the protein AIM (apoptosis inhibitor of macrophage, also known Spα, Api6, and CD5L) in the context of its effects on adipocytes, because AIM is produced and secreted specifically by tissue macrophages, and its expression in vivo is markedly increased with obesity progression in mice (Miyazaki et al., 1999; Arai et al., 2005).

The AIM protein is a member of the scavenger receptor cysteine-rich superfamily (SRCR-SF) and was initially identified as an apoptosis inhibitor that supports the survival of macrophages themselves against various apoptosis-inducing stimuli (Miyazaki et al., 1999). As a secreted molecule, AIM has been detected in human and mouse blood at varying levels (Miyazaki et al., 1999; Gebe et al., 1997, 2000; Gangadharan et al., 2007; Kim et al., 2008; Gray et al., 2009). Based on the observation that *AIM* is a direct target for regulation by nuclear receptor LXR/RXR heterodimers (Joseph et al., 2004; Valledor et al., 2004), we found that AIM is expressed in lipid-laden macrophages at atherosclerotic lesions, and this induction is associated with atherosclerogenesis by supporting the survival of macrophages within lesions (Arai et al., 2005). Other studies have shown that AIM appears to be multifunctional and is effective in cell types other than macrophages, including B and natural killer (NK) T lymphocytes (Yusa et al., 1999; Kuwata et al., 2003) and myeloid cells (Qu et al., 2009). However, the functional nature of AIM remains enigmatic because we are ignorant of the precise mechanism by which it elicits its effects.

In the present study, we assessed the expression of AIM by adipose tissue macrophages in obese mice. We also analyzed how AIM interacts with adipocytes. In addition, an effect of AIM on adipocytes and its consequence with respect to the regulation of adipocyte size in vivo was determined. Finally, we investigated the molecular mechanism underlying this role of AIM in adipocytes. Based on these results, we will discuss the putative role of AIM on the state of adipose tissues.

RESULTS

AIM in Adipose Tissue Macrophages in Obese Mice

We first assessed the expression of AIM by adipose tissue macrophages in obese C57BL/6 (B6) mice after the administration of a high-fat diet (HFD) (fat kcal 60%) for 20 weeks. In obese mice, large numbers of macrophages were observed within visceral fat tissues, forming clusters or crown-like structures (CLSs) (Cinti et al., 2005), whereas few adipose tissue macrophages were detected in lean mice (Figure 1A). As shown in Figure 1B, macrophages (stained with F4/80 pan macrophage antibody) in obese adipose tissues showed staining with an antibody specific to AIM (SA-1) (Arai et al., 2005). These AIM-positive macrophages were also positive for interleukin (IL)-6 staining, indicating that they were the inflammatory macrophage type (M1) (Figure 1B). In contrast, F4/80-positive macrophages within adipose tissues from lean mice were negative for AIM and IL-6 staining (Figure 1B). Similarly, the serum level of AIM was increased in obese mice compared to lean mice (Figure 1C). It is possible that AIM detectable in lean mice is derived predominantly from macrophages in other macrophage-containing tissues (Miyazaki et al., 1999; Gebe et al., 2000; Arai et al., 2005). To exclude the possible expression of AIM by adipocytes, adipocytes from epididymal fat tissue of obese mice were fractionated after collagenase treatment (Brake et al., 2006) and assessed for *AIM* expression by quantitative real-time PCR (QPCR). No *AIM* expression was observed in purified adipocytes (Figure S1A). In addition, 3T3-L1 adipocytes were analyzed after the induction of maturation by insulin, dexamethasone (DEX), and isobutylmethylxanthine (IBMX). Again, *AIM* expression was not detectable in mature 3T3-L1 adipocytes (Figure S1B).

Endocytosis of AIM into Adipocytes

Intriguingly, although we found no *AIM* expression by adipocytes (Figure S1), some adipocytes surrounding adipose tissue macrophages in obese mice showed AIM staining (Figure 2A, arrows). This may indicate a physiologic association of AIM with tissue adipocytes. To test this possibility, we injected recombinant AIM (rAIM) into epididymal fat in obese male $AIM^{-/-}$ mice and analyzed fat tissue histologically 3 hr later. Epididymal fat was selected for this experiment owing to its ease of manipulation. Interaction of AIM with adipocytes was clearly confirmed in $AIM^{-/-}$ mice. As shown in Figure 2B (left and middle lanes), $AIM^{-/-}$ adipocytes were positive for AIM staining when rAIM was injected locally into fat tissue (Figure 2B, left and middle lanes). Staining for AIM was also detected in adipocytes in fat tissue in which rAIM was administered systemically to $AIM^{-/-}$ mice via intravenous (i.v.) injection (Figure 2B, right lane). These results implicate adipocytes as a target cell type for AIM. Macrophages also stained for AIM in $AIM^{-/-}$ adipose tissue after injection of rAIM (Figure 2B), consistent with the fact that AIM is effective in macrophages (Miyazaki et al., 1999; Arai et al., 2005).

To further investigate how AIM interacts with adipocytes, differentiated 3T3-L1 adipocytes were treated with rAIM, and the association of rAIM with these cells was analyzed by confocal microscopy. Interestingly, rAIM accumulated within the cytoplasm of adipocytes, forming many dots within the intracellular compartment (Figure 3A). After stimulation with insulin, DEX, and IBMX, a large proportion of 3T3-L1 cells underwent differentiation, expressing peroxisome proliferator-activated receptor γ 2 (PPARγ2) at a high level, whereas some cells remained in an undifferentiated state, expressing PPARγ2 at a low or undetectable level (Madsen et al., 2003). As shown in Figure 3A, among this heterogeneous cell population, mature adipocytes strongly positive for PPARγ2 (yellow arrows) efficiently incorporated rAIM, whereas adipocytes faintly positive for PPARγ2 (blue arrows) or negative (white arrows) did not (left and middle lanes). Preadipocytes not stimulated by insulin, DEX, and IBMX did not incorporate rAIM (Figure 3A, right lane). As shown in Figure 3B, incorporated rAIM colocalized with early endosomes (positive for early endosome antigen 1; EEA1) but not with late endosomes (positive for Rab7) or recycling endosomes (positive for Rab11). These results suggest that incorporated AIM was transported to the cytosol during endosome maturation. No costaining for AIM and lysosomes or lipid droplets was observed (Figure 3B; AIM + lysosome, AIM + lipid droplets). Additional analysis of the cells by electron microscopy shown may support the specific colocalization of AIM with endosomes (Figures 3C and S2). Gold particles indicating rAIM immunoreactivity were mainly associated with endosome-like structures, where the limiting membrane of the structures and the periphery of their contents were heavily labeled (Figure 3C). Endocytosis of rAIM was observed at the cell membrane (Figure 3C, indicated by arrows). Other organelles were essentially negative for AIM immunolabeling (Figure S2). All these data suggest that AIM is incorporated into adipocytes via endocytosis, is transported to the cytoplasm, and function intracellularly.

Cell-Surface CD36-Mediated Internalization of AIM

The accumulation of AIM at the membrane of endosome-like particles (Figure 3C) indicates that the internalization of exogenous AIM may be mediated by a cell-surface molecule. As a candidate molecule responsible for endocytosis, we focused on scavenger receptor CD36 because it promotes the internalization of various molecules, including lipoproteins and fatty acids (Greenwalt et al., 1992; Ibrahimi and Abumrad, 2002), and it is expressed by adipocytes and macrophages, which are target cells for AIM. Thus, we assessed whether treatment of 3T3-L1 adipocytes with a neutralizing antibody against CD36 (clone JC63.1; mouse IgA) interfered with rAIM uptake. As shown in Figure 3D, incorporation of rAIM was drastically decreased in the presence of this neutralizing antibody. In addition, we injected rAIM intravenously into $CD36^{-/-}$ (Febbraio et al., 1999) and $CD36^{+/+}$ mice and analyzed the incorporation of rAIM into adipose tissues. As shown in Figure 3E, incorporation of rAIM into adipocytes was markedly less in $CD36^{-/-}$ mice compared to $CD36^{+/+}$ mice. These data strongly indicate that CD36 is responsible for AIM internalization. This was also supported by microscopic analysis of the association of rAIM

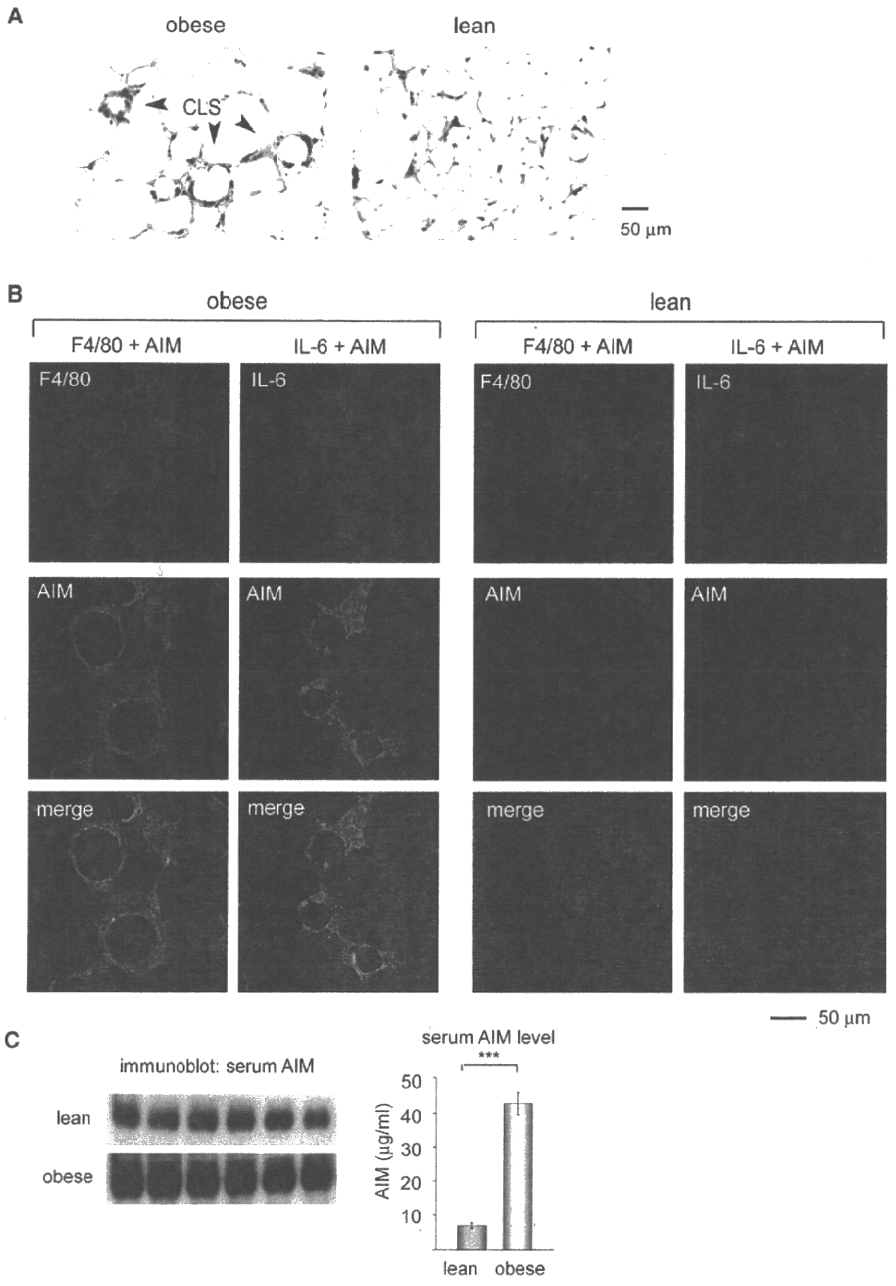

Figure 1. Immunohistochemical Analysis of AIM in Adipose Tissues

(A) Representative photomicrographs of visceral fat tissue from lean (fed with normal chow) or obese (fed with a HFD for 20 weeks) wild-type B6 mice stained with hematoxylin and eosin (H&E). The crown-like structures (CLSs) formed by recruited macrophages are indicated by arrows.

(B) Specimens of visceral fat tissues from lean or obese B6 mice were costained for AIM (green) and F4/80 (pan macrophage marker; red) or AIM (green) and IL-6 (red).

(C) Immunoblotting for serum AIM. A volume of 1 μl of serum from six separate lean (fed with normal chow) or obese (fed with a HFD for 20 weeks) mice was used. Results for immunoblots and actual AIM concentration are presented. AIM concentration was calculated by comparison with the density obtained with various amounts of recombinant AIM (rAIM) on the same blot. The density of the signal was calculated using image analysis software NIH ImageJ. Error bar indicates SEM.

with Flag-tagged mouse CD36 expressed on the surface of HEK293T cells. Notably, the accumulation of rAIM staining (green) was specifically colocalized with Flag-CD36 (red) on the cell surface (Figure S3).

AIM Decreases Adipocyte Lipid Droplet Size

We next assessed the effect of incorporated AIM in host adipocytes. To achieve this, differentiated 3T3-L1 adipocytes in culture (at 4 days after maturation stimulation) were challenged

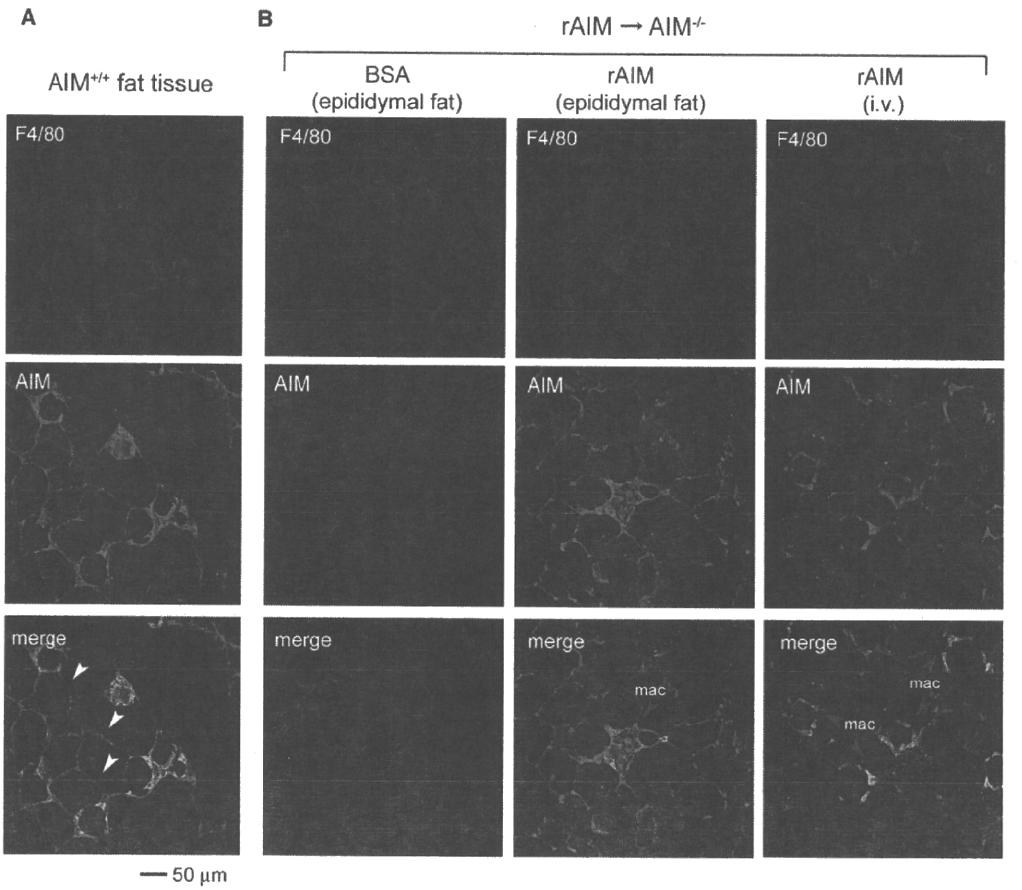

Figure 2. Association of Exogenous AIM with Adipocytes

(A) Epididymal fat sections were stained for AIM (green) and F4/80 (red). Staining for AIM was detected in macrophages and some adipocytes (arrows).

(B) Uptake of rAIM by $AIM^{-/-}$ adipocytes in vivo. $AIM^{-/-}$ mice were injected with rAIM (middle lane) or BSA (left lane) directly into the epididymal fat (total 100 μg for each at several loci) or with rAIM systemically (300 μg) via i.v. injection (right lane). Three hours after injection, tissue sections were generated and stained for AIM (green) and macrophage F4/80 (red). mac: macrophage.

with rAIM. Remarkably, the size of lipid droplets within the cells was decreased after a 6 day incubation of cells with rAIM (Figure 4A). In addition, the number of cells containing lipid droplets was also decreased (Figure 4A). Supernatant viscosity was also markedly enhanced by the administration of rAIM. These results suggest that rAIM induced a lipolytic response, resulting in the liberation of droplet components such as glycerol and fatty acids from the cells (Zechner et al., 2005; Duncan et al., 2007). We tested this possibility by determining the efflux of glycerol and free fatty acids (FFAs) on days 2, 4, and 6 after stimulation with rAIM. As shown in Figure 4B, the amount of glycerol and FFAs in the supernatant increased significantly when adipocytes were maintained in rAIM. In vivo, basal levels of FFA and glycerol in serum were lower in $AIM^{-/-}$ obese mice than in $AIM^{+/+}$ obese mice (Figure 4C), consistent with the in vitro results.

mRNA levels for *fat-specific protein 27* (*FSP27*, also termed *cidec*), *Perilipin*, and *Adipophilin*, important elements involved in the formation of lipid droplets (Ducharme and Bickel, 2008; Puri and Czech, 2008), were decreased after treatment of 3T3-L1 adipocytes with rAIM (Figure 4D). A significant decrease in these mRNA levels was already apparent 2 days after challenge with rAIM (Figure 4D), consistent with the progression of lipolysis, as reported previously (Zechner et al., 2005; Nishino et al., 2008). In contrast, mRNA level of mature adipocyte markers such as *PPARγ2*, *CCAAT-enhancer-binding protein α* (*C/EBPα*), and *glucose transporter 4* (*GLUT4*) and an immature adipocyte marker, *Preadipocyte factor-1* (*PREF-1*) (Smas and Sul, 1993), was not remarkably changed in response to rAIM treatment, suggesting that rAIM did not appear to induce dedifferentiation of adipocytes (Figure 4D). Local injection of rAIM into epididymal fat tissue of $AIM^{-/-}$ mice resulted in similar changes in mRNA levels of these genes (Figure 4E).

Increase in Adipocyte Size and Adipose Tissue Mass in $AIM^{-/-}$ Mice

Consistent with the observations in 3T3-L1 cells, the size of visceral fat adipocytes was larger in obese $AIM^{-/-}$ mice than in obese $AIM^{+/+}$ mice (Figure 5A). Relevant to this enlargement of

adipocytes, the increase in weight of both visceral and subcutaneous fat tissues in mice fed with a HFD (12 weeks) was more accelerated in *AIM*$^{-/-}$ mice than in *AIM*$^{+/+}$ mice (Figure 5B). This difference was also apparent in mice fed with a HFD for a longer period (20 weeks) (Figure S4). It is noteworthy that *AIM*$^{-/-}$ mice and *AIM*$^{+/+}$ mice fed with a HFD showed comparable metabolic rates (e.g., body temperature, oxygen consumption, and food intake) (Figure S5). Locomotor activity was also equivalent in both types of mice (Figure S5). Thus, AIM appears to influence adipose tissue mass by specifically affecting adipocytes.

We also injected rAIM intraperitoneally (twice a week) into *AIM*$^{-/-}$ mice fed with a HFD for 5 weeks to assess whether rAIM administration might suppress the increase in adipose tissue mass. As expected, the increase in weight of whole-body as well as both visceral and subcutaneous fat tissues was significantly less in mice injected with rAIM than in those injected with bovine serum albumin (BSA) (Figure 5C). As observed for the treatment of 3T3-L1 adipocytes with rAIM (Figure 4D), mRNA levels of *FSP27*, *Perilipin*, and *Adipophilin* were also lower in the epididymal adipose tissue in mice injected with rAIM (Figure 5D). Interestingly, mRNA level of *PREF-1* was higher in rAIM-injected mice, although that of *PPARγ2*, *C/EBPα*, or *GLUT4* was similar in mice injected with rAIM or BSA (Figure 5D).

AIM Decreased Fatty Acid Synthase Activity

We were interested in the intracellular target molecule(s) of incorporated AIM in adipocytes. To this end, we performed immunoprecipitation-mass spectrometry (IP-MS) analysis with lysates from different cells and tissues. Fatty acid synthase (FAS) was identified as a candidate molecule with the potential to associate with AIM (other proteins, including carbamoyl phosphate synthase-1, major vault protein, and aldehyde dehydrogenase 1 family member L1, were also associated with AIM; complete results of this analysis will be published elsewhere). FAS is highly expressed in adipose tissues and catalyzes the synthesis of saturated fatty acids, such as palmitate, from acetyl-CoA and malonyl-CoA precursors. Accumulating evidence has highlighted critical roles of FAS in a variety of biological aspects, including early embryogenesis (Chirala et al., 2003), in addition to providing a metabolic substrate. A number of biochemical and genetic studies have suggested the involvement of FAS in the regulation of adipose tissue mass (Loftus et al., 2000; Makimura et al., 2001; Kumar et al., 2002; Mobbs and Makimura, 2002; Shimokawa et al., 2002; Kovacs et al., 2004; Liu et al., 2004; Ronnett et al., 2005; Schmid et al., 2005; Chakravarthy et al., 2009a).

We confirmed the association of AIM and FAS in vivo and in vitro. After injecting rAIM into epididymal fat of obese *AIM*$^{-/-}$ mice, we precipitated incorporated rAIM from fat tissue lysates and addressed whether endogenous FAS was also precipitated. As shown in Figure 6A, the proteins coprecipitated, confirming the association of incorporated AIM and cytosolic FAS. In addition, a coimmunoprecipitation (coIP) assay with HEK293T cells expressing Flag-tagged FAS and HA-tagged AIM showed that the two proteins coprecipitated, indicating that AIM possesses the potential to bind to FAS (Figure 6B).

We also attempted to map FAS-binding region(s) for AIM. FAS consists of seven discrete functional domains: ketoacyl synthase (KS), malonyl/acetyl transferase (MAT), dehydrase (DH), enoylreductase (ER), ketoreductase (KR), acyl carrier protein (ACP), and thioesterase (TE) (Smith, 1994). There is a central core (CC) between the DH and ER domains that has no known catalytic function and may play a structural role in stabilizing the dimer (illustrated in schematic in Figure 6C). We assessed the association of HA-tagged AIM with each FAS region tagged with a Flag sequence by coIP assay. Notably, AIM bound specifically to ER, DH, TE, and CC domains, but not to the N-terminal region containing KS and MAT, which are involved in the initial acyl chain assembly (i.e., condensation of acetyl and malonyl moieties to 3-ketobutyryl-ACP along with the release of CO_2) (Figures 6C and S6). Thus, AIM appears to influence the elongation of fatty acid chains (which involves ER and DH) and the release of synthesized palmitate (which is dependent on TE).

The association of AIM with the CC domain suggested that AIM might also affect the dimerization of FAS. It is well known that FAS is highly functional as a dimerized form, whereas monomeric FAS possesses little or no activity (Smith et al., 1985; Asturias et al., 2005). Therefore, we analyzed the dimer/monomer status of FAS protein in 3T3-L1 adipocytes after culture in the presence or absence of rAIM for 6 days. As expected, the proportion of dimerized FAS (500 kDa) (as assessed by separation of FAS on a Tris-acetate gel specific for large molecular weight proteins) was significantly less in cells maintained in the presence of rAIM than in cells without rAIM treatment (Figure 6D).

Consistent with these results, the enzymatic activity of FAS (as assessed by the consumption of malonyl-CoA) (Kelley et al., 1986) was markedly decreased in 3T3-L1 adipocytes treated with rAIM as above (Figure 6E). The decrease in FAS activity induced by rAIM (5 μg/ml) was at a similar level to that induced by C75, a specific FAS inhibitor (Kuhajda et al., 2000), when used at a functional concentration (25 μM) (Figure 6E). In vivo, FAS activity was significantly increased in epididymal fat of *AIM*$^{-/-}$ mice compared to that of *AIM*$^{+/+}$ mice (Figure 6F). In addition, supplementation of rAIM via direct injection decreased FAS activity in epididymal fat of *AIM*$^{-/-}$ mice (Figure 6G).

AIM and FAS Inhibitor C75 Showed Comparable Effects on Adipocytes

To address whether the effect of AIM on adipocytes resulted from the suppression of FAS activity, we tested whether treatment of 3T3-L1 adipocytes with AIM or FAS inhibitor C75 had similar consequences. As expected, rAIM (5 μg/ml) and C75 (25 μM) induced an increase in the efflux of glycerol and FFAs at comparable levels (Figure 7A). We also assessed the influence of AIM on adipogenesis, because Schmid et al. (2005) reported that inhibition of FAS prevented preadipocyte differentiation. Interestingly, the presence of rAIM during stimulation by insulin, DEX, and IBMX (48 hr) completely prevented differentiation of 3T3-L1 preadipocytes toward mature adipocytes at a level equivalent to that observed with C75 (Figure 7B). The numbers of dead cells did not increase in the presence of rAIM at different time points, as assessed by staining with trypan blue or propidium iodide (data not shown). This excludes the argument that rAIM might induce death of 3T3-L1 cells, appearing to decrease the overall number of mature adipocytes. In addition, AIM did not simply attenuate either (or all) of the three stimulators via

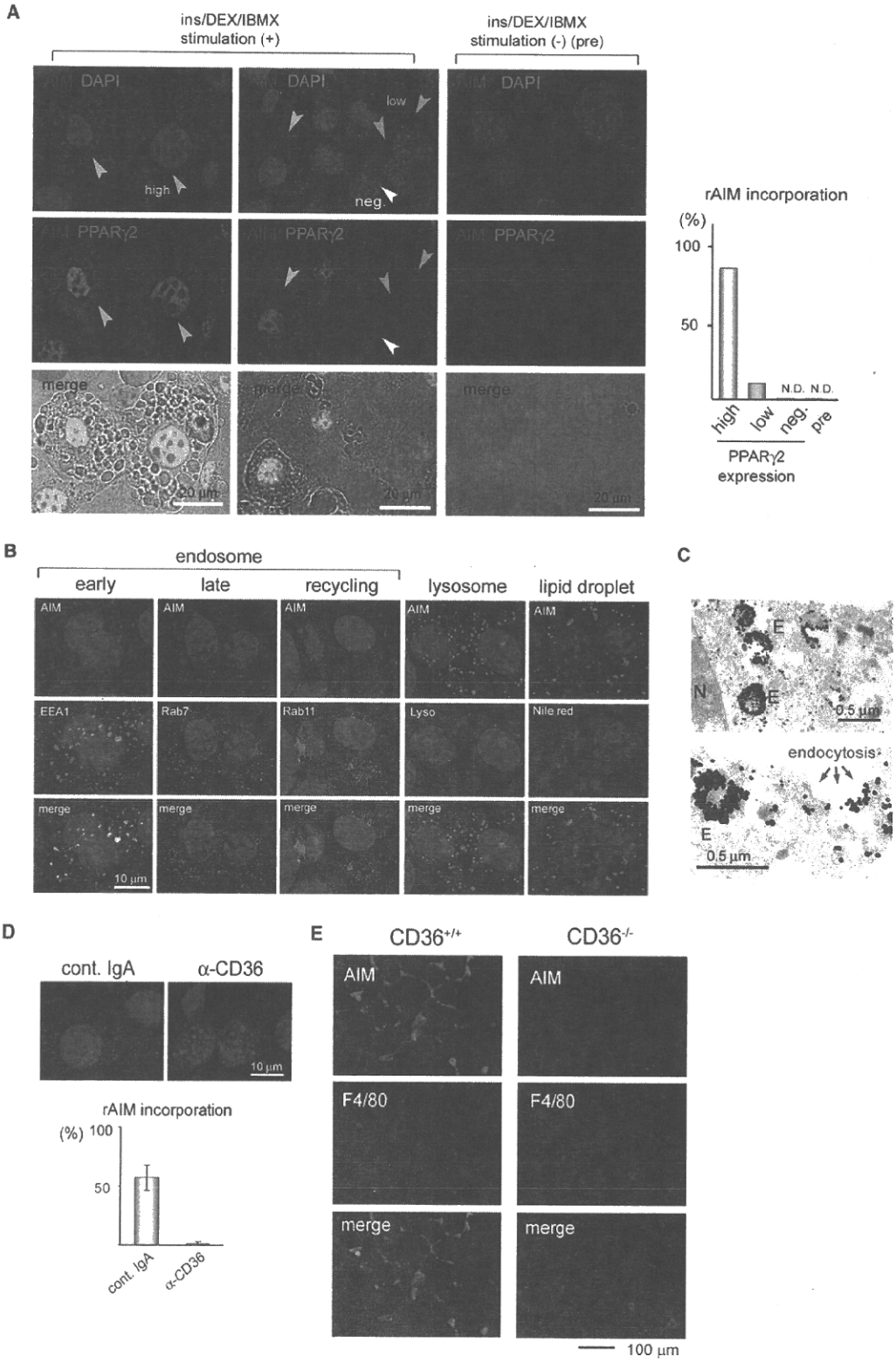
A
ins/DEX/IBMX stimulation (+)
ins/DEX/IBMX stimulation (-) (pre)
DAPI
high
low
neg.
PPARγ2
merge
20 μm
rAIM incorporation
(%)
100
50
N.D. N.D.
high
low
neg.
pre
PPARγ2 expression
B
endosome
early
late
recycling
lysosome
lipid droplet
AIM
EEA1
Rab7
Rab11
Lyso
Nile red
merge
10 μm
C
E
N
0.5 μm
endocytosis
D
cont. IgA
α-CD36
10 μm
rAIM incorporation
(%) 100
50
cont. IgA
α-CD36
E
CD36+/+
CD36-/-
AIM
F4/80
merge
100 μm